

A Balanced Budget View on Forming Giant Planets by Pebble Accretion

Jonathan W. Lin^{1,2*}, Eve J. Lee^{1,3†}, Eugene Chiang^{1,4‡}

¹Department of Astronomy, University of California Berkeley, Berkeley, CA 94720-3411, USA

²Department of Engineering Science, University of California Berkeley, Berkeley, CA 94720-1702, USA

³TAPIR, Walter Burke Institute for Theoretical Physics, Mailcode 350-17, Caltech, Pasadena, CA 91125, USA

⁴Department of Earth and Planetary Science, University of California Berkeley, Berkeley, CA 94720-4767, USA

ABSTRACT

Pebble accretion refers to the assembly of rocky planet cores from particles whose velocity dispersions are damped by drag from circumstellar disc gas. Accretion cross-sections can approach maximal Hill-sphere scales for particles whose Stokes numbers approach unity. While fast, pebble accretion is also lossy. Gas drag brings pebbles to protocores but also sweeps them past; those particles with the largest accretion cross-sections also have the fastest radial drift speeds and are the most easily drained out of discs. We present a global model of planet formation by pebble accretion that keeps track of the disc's mass budget. Cores, each initialized with a lunar mass, grow from discs whose finite stores of mm–cm sized pebbles drift inward across all radii in viscously accreting gas. For every $1M_{\oplus}$ netted by a core, more than $\sim 30M_{\oplus}$ are lost to radial drift. Core growth rates are typically exponentially sensitive to particle Stokes number, turbulent Mach number, and solid surface density. This exponential sensitivity tends to generate binary outcomes: either sub-Earth cores remain sub-Earth, or explode into Jupiters, with the latter migrating inward to varying degrees. When Jupiter-breeding cores assemble from mm–cm sized pebbles, they do so in discs where such particles drain out in $\sim 10^5$ yr or less; such fast-draining disks do not fit mm-wave observations.

Key words: planets and satellites: formation

1 INTRODUCTION

Gas giant planets can only form when there is still enough gas in their natal environments, i.e., when circumstellar discs are young and gas-rich. The core accretion paradigm of gas giant formation plays out in three phases (Pollack et al. 1996). Phase 1: a rocky core coagulates from disc solids. Phase 2: a gaseous envelope forms around the core, fed from the ambient disc at a rate regulated by internal cooling and contraction of the envelope. Phase 3: the planet inflates into a gas giant as the gas accretion rate onto the core “runs away” in response to the envelope’s self-gravity.

Of these three phases, perhaps the first is the least understood. There is a need for gravitational focussing of collisions between solid particles, as timescales for coagulating a Jupiter-breeding core (having \gtrsim a few Earth masses) at the stellocentric distances where Jupiters are found (a few AU) are orders of magnitude longer than the 1–10 Myr life-

times of gas discs—if collision cross-sections are only geometric and not enhanced by gravity (Goldreich et al. 2004). How much collisions are focussed depends on much particle velocity dispersions are damped, which in turn depends on particle size distributions. These factors are not known. The problem is tied up with the longstanding mystery of planetesimal formation (Chiang & Youdin 2010).

“Pebble accretion” makes inroads on the problem of core assembly by exploiting the ability of seed cores to attract particles small enough to have their velocity dispersions damped by aerodynamic drag from the ambient gas disc (for a comprehensive review, see Ormel 2017). Without addressing the question of the origin of the seed core (seeds as low in mass as $\sim 10^{-3}M_{\oplus}$ have been assumed), the theory of pebble accretion points out that for particles whose aerodynamic stopping times are comparable to orbital times—“pebbles” with order-unity Stokes numbers—the accretion cross-section can approach its maximum value set by the Hill sphere of the seed core. Assembly times of Jupiter-breeding cores have been reported to range from $\sim 10^4$ yr (Lambrechts & Johansen 2012) to $\sim 10^6$ yr (Lambrechts & Johansen 2014). Pebble accretion has been hailed as a key

* Contact e-mail: jon.880@berkeley.edu

† evelee@caltech.edu

‡ echiang@astro.berkeley.edu

Jupiter Formation by Pebble Accretion

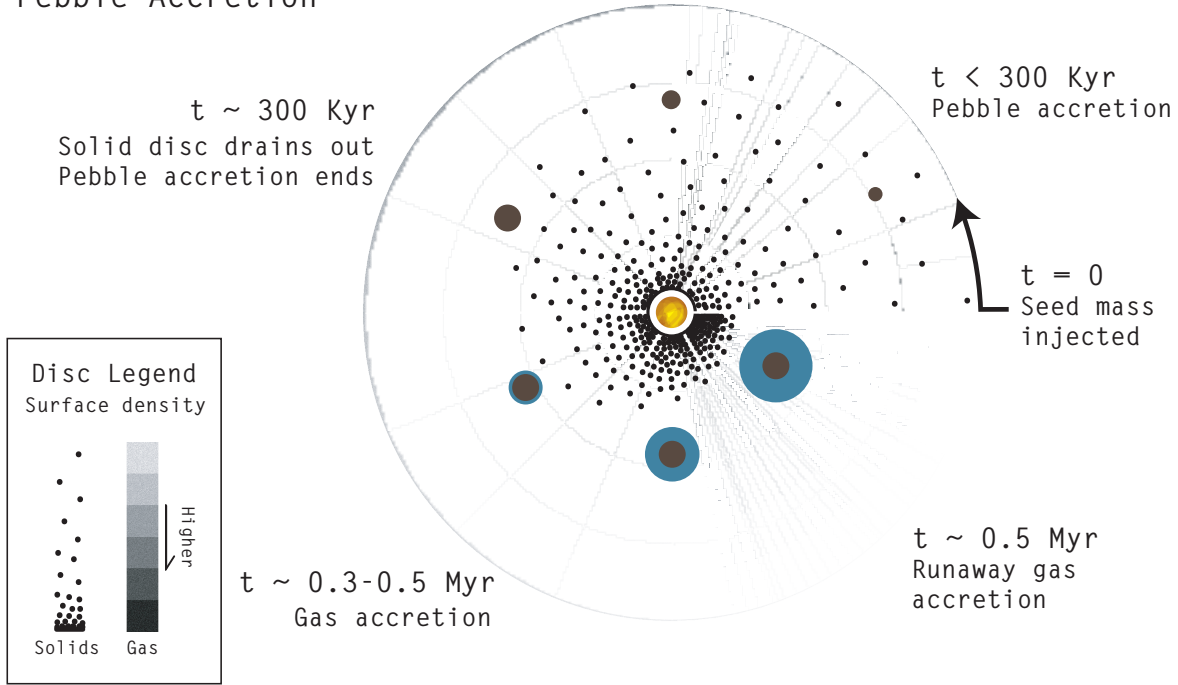


Figure 1. An example formation pathway for Jupiters, abstracted from the quantitative model shown in Figure 8. Each sector represents a different temporal snapshot of the disc and planet, to be read counterclockwise starting from 3 o’clock. A seed core (brown) is placed in a model gas disc (grey) and begins accreting solid particles (“pebbles”; black). At the same time that pebbles feed the core, they drift inward by aerodynamic drag exerted by the ambient gas disc. The core stops growing once the outer edge of the solid disc sweeps by. When core assembly ends and heating from pebble accretion subsides, a gas envelope (blue) grows by Kelvin-Helmholtz cooling and contraction. Eventually, the planet’s gas mass becomes comparable to its core mass, the atmosphere’s cooling time shortens catastrophically because of atmospheric self-gravity, triggering runaway gas accretion and inflating the planet into a gas giant. Concurrent with these processes are the inward migration of the planet and the dispersal of the gas disc (driven by viscous accretion in our model).

ingredient in understanding various architectural features of planetary systems, both in Solar and extrasolar contexts, including: the dichotomy between inner terrestrial planets and outer giants (Morbidelli et al. 2015; Levison et al. 2015); the preponderance of gas giants at a few AU and of ice giants beyond (Bitsch et al. 2015a,b); the orbital period distribution of warm Jupiters (Ali-Dib et al. 2017); and the mass distribution of planets in the TRAPPIST-1 system (Ormel et al. 2017).

Although pebble accretion is touted for its speed, it is perhaps less appreciated that it can be lossy. The same aerodynamic drag that brings pebbles into contact with cores also sweeps them past, as part of the background radial drift of solids from the outer to the inner disc (e.g., Weidenschilling 1977). Particles that are most easily accreted, with Stokes numbers near unity, also drift the fastest toward the star. Factoring in this background flow—tallying how many Earth masses flow under the bridge for every Earth mass netted—is one aim of this paper. We study how pebble accretion plays out in a global (1D in radius), fully time-dependent model, one that keeps track of the disc’s finite mass budget while growing a core. We consider pebble sizes ranging from 0.01–1 cm, like those probed by mm–cm wavelength images of protoplanetary discs (e.g., ALMA Partnership et al. 2015; Andrews et al. 2016), and near the

maximum size that might be achievable by particle-particle sticking (Chiang & Youdin 2010, their section 4). Aside from specifying a few model inputs such as the disc’s initial solid mass, its gas mass, and its Shakura-Sunyaev α , we make no assumption about the regime of pebble accretion that a protocore finds itself in, letting system parameters dictate which of the myriad cases outlined by Ormel & Klahr (2010) is appropriate at any given time. In addition to solving the equations of pebble accretion, the model also accounts for gas accretion onto cores, and orbital migration of planets by disc torques. Our goal is to assess more realistically the prospects of pebble accretion at forming various kinds of planets—Earths, Neptunes (a.k.a. super-Earths), and Jupiters—in discs resembling those observed. We describe our model in section 2, present results in section 3, and summarize and look to the future in section 4.

2 MODEL

We construct a global (1D in disc radius) model of planet formation. Figure 1 presents a pictorial overview. The model tracks the evolution of a viscous gas disc (section 2.1); the radial transport of solid particles of fixed size (section 2.2); the assembly of a single rocky core by pebble accretion (section 2.3); the lowering of disc gas density near the planet’s

orbit due to gap opening (section 2.4); how the core stops accreting solids (section 2.5); how cores that have stopped accreting solids subsequently accrete nebular gas (sections 2.6 and 2.7); and migration of the nascent planet (section 2.8). Readers interested in a bare-bones technical summary of the underlying equations and values of input parameters can jump to section 2.9. Table 1 lists our symbols and their meanings.

2.1 The Gas Disc

To model the gas surface density Σ_g as a function of radius a and time t , we adopt the similarity solution for an isolated, viscously spreading disc (Lynden-Bell & Pringle 1974; Hartmann et al. 1998):

$$\Sigma_g(a, t) = \frac{Ca_1}{3\pi\nu_1 a} \mathcal{T}^{-3/2} \exp\left[\frac{-a/a_1}{\mathcal{T}}\right] \quad (1)$$

where a_1 is a fiducial radius, $\nu_1 = \nu(a_1)$ is the kinematic viscosity at a_1 , $\mathcal{T} = t/t_s + 1$, and

$$t_s = \frac{a_1^2}{3\nu_1} \quad (2)$$

is a measure of the viscous diffusion time at a_1 . Equation (1) presumes that the disc viscosity scales as

$$\nu = \alpha c_s H \propto a^1 \quad (3)$$

for sound speed c_s , scale height $H = c_s/\Omega$, orbital angular frequency Ω , and dimensionless viscosity parameter α (Shakura & Sunyaev 1973). The scaling of (3) follows, in turn, from an assumed temperature profile

$$T = T_0 \left(\frac{a}{a_0}\right)^{-1/2} \quad (4)$$

for $a_0 = 1$ AU and $T_0 = 260$ K. The normalization constant C depends on an assumed initial gas mass of the disc $M_{\text{disc},g}(0)$. Given (4), the disc aspect ratio is

$$H/a = 0.032 \left(\frac{a}{a_0}\right)^{1/4}. \quad (5)$$

In sum, there are three free parameters: $M_{\text{disc},g}(0)$, α , and a_1 (equivalently, t_s). The ranges of these and other variables are given in Table 1.

2.2 The Solid Disc

We follow the contraction of the solid disc as its constituent particles drift inward by gas drag. In inertial space, particles travel radially inward at a speed

$$v_{\text{drift}} = \frac{3\nu}{2a} \frac{1}{1+\tau^2} + 2v_{\text{hw}} \frac{\tau}{1+\tau^2} \quad (6)$$

where $3\nu/(2a)$ is the steady-state viscous gas velocity, v_{hw} is the azimuthal headwind velocity experienced by particles in pressure-supported gas, and $\tau = \Omega_{\text{stop}}$ is the dimensionless particle stopping time (a.k.a. Stokes number). Equation (6) generalizes equation (13) of Chiang & Youdin (2010). The headwind velocity is

$$v_{\text{hw}} = -\frac{c_s^2}{2\Omega a} \frac{\partial \log P_g}{\partial \log a}, \quad (7)$$

where the gas pressure P_g and density ρ_g are approximated as

$$P_g = \rho_g c_s^2 = \frac{\Sigma_g}{H} c_s^2. \quad (8)$$

The particle stopping time is

$$\tau = \begin{cases} \frac{\Omega \rho_s s}{\rho_g c_s} & s < \frac{9}{4} \lambda \\ \frac{4\Omega \rho_s s^2}{9\rho_g c_s \lambda} & s > \frac{9}{4} \lambda \end{cases} \quad \begin{array}{l} (\text{Epstein drag}) \\ (\text{Stokes drag}) \end{array} \quad (9)$$

where s is the particle radius, $\rho_s = 1 \text{ g/cm}^3$ is the internal density of a single particle, and $\lambda = 4 \times 10^{-9}/\rho_g$ is the gas mean free path in cgs units. For simplicity we take s to be strictly constant in a given model (cf. Ormel & Kobayashi 2012 who relax this assumption).

The radial transport of solids—i.e., the evolution of solid surface density $\Sigma_s(a)$ with t —is solved using a simple Lagrangian scheme. At $t = 0$, the solid disc, of total mass $M_{\text{disc},s}(0)$, is divided into 1000 concentric rings that are logarithmically spaced from $a_{\text{in}} = 0.01$ AU to $a_{\text{out}}(0) = a_1$. Mass is assigned to each ring such that the initial solid surface density scales as a^{-1} (following the viscously relaxed portion of the gas disc; section 2.1). Each ring conserves its mass (the mass lost to pebble accretion onto the planetary core is negligible) but has its radial boundaries evolved according to equation (6). The evolution of the ring boundaries is solved using a fourth-order Runge-Kutta scheme from $t = 10^{-3}$ Myr to 100 Myr over 5000 logarithmically spaced timesteps. The solid surface density of each ring is simply the ring mass divided by the (evolving) ring area. A ring whose inner boundary crosses inside a_{in} has its inner boundary held at a_{in} and its surface density fixed thereafter; once the ring's outer boundary crosses a_{in} , the ring is removed from the calculation. To reduce numerical noise when calculating Σ_s for a given orbital radius a of the core, we use cubic splines to interpolate over the solid surface densities of up to 10 rings inside a , plus up to 10 rings outside (hitting disc boundaries can limit the number of rings used in the interpolation). Because the innermost ring is handled differently as per the above, it is not used in any interpolation, and if the core falls within the innermost ring, its local Σ_s is simply that of that ring.

A sample evolution of $\Sigma_s(a, t)$ is shown in Figure 2. The solid disc introduces two free parameters, the particle size s and the initial total solid mass $M_{\text{disc},s}(0) \equiv Z M_{\text{disc},g}(0)$ (see Table 1).

2.3 Core Formation by Pebble Accretion

To grow cores starting from an assumed seed mass of $M_{\text{core}}(0) = 10^{-2} M_{\oplus}$, we follow the pebble accretion prescriptions of Ormel & Klahr (2010, OK10), augmenting their formulae to account for gas turbulence (see also Ormel & Liu 2018 and Rosenthal et al. 2018 who provide a more general treatment of stochasticity in pebble accretion). A core embedded in a disc of solids accretes mass at a rate

$$\dot{M}_{\text{core}} = 2\Sigma_s R_{\text{acc}} v_{\text{acc}} \times \min(1, R_{\text{acc}}/H_s) \quad (10)$$

where particles that come within a distance R_{acc} of the core, moving at velocity v_{acc} relative to the core, are accreted. According to (10), when R_{acc} (the accretion “cross section”

Table 1. Model Parameters

Used for	Symbol	Description	Values	Reference
Gas disc	α	Viscosity parameter / turbulent Mach number	$10^{-4}, 10^{-3}, 10^{-2}$	Section 2.1
	a_1	Characteristic disc radius	10, 100 AU	Section 2.1
	$M_{\text{disc,g}}(0)$	Initial mass of gas disc	10, 100 M_J	Section 2.1
	T	Disc temperature	$260 \text{ K} \times (a/1 \text{ AU})^{-1/2}$	Section 2.1
Solid disc	a_{in}	Inner radius of the solid disc	0.01 AU	Section 2.2
	$a_{\text{out}}(0)$	Initial outer radius of the solid disc	a_1	Section 2.2
	s	Pebble radius	0.01, 0.1, 1 cm	Section 2.2
	Z	Solid-to-gas mass ratio $M_{\text{disc,s}}(0)/M_{\text{disc,g}}(0)$	0.003, 0.009, 0.031	Section 2.2
Core	$a(0)$	Initial core orbital radius	0.1, 0.3, 1, 3, 10, 30 AU	Section 2.9
	$M_{\text{core}}(0)$	Initial seed core mass	$0.01 M_{\oplus}$	Section 2.9
	$M_{\text{gas}}(0)$	Initial planet gas mass	0	Section 2.9

Notes: (a) In selecting model parameters, we ensure that the initial core orbital radius $a(0)$ is strictly less than the characteristic disc radius a_1 . In total, we have 540 unique parameter combinations. (b) Initial solid disc masses $M_{\text{disc,s}}(0) = Z M_{\text{disc,g}}(0) \in \{10, 30, 100, 300, 1000\} M_{\oplus}$ (only 5 unique values of $M_{\text{disc,s}}(0)$ corresponding to 6 unique combinations of $M_{\text{disc,g}}(0)$ and Z).

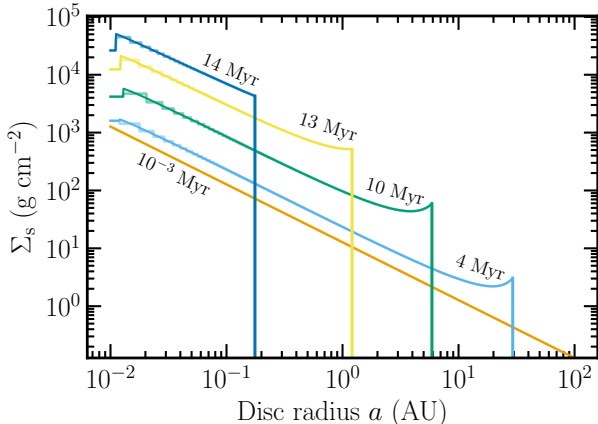


Figure 2. Surface density of solids, evolved according to our Lagrangian ring scheme (section 2.2), for a disc with $\alpha = 10^{-4}$, $a_1 = 100 \text{ AU}$, $s = 0.01 \text{ cm}$, $M_{\text{disc,g}}(0) = 100 M_J$, and $M_{\text{disc,s}}(0) = 300 M_{\oplus}$ (note that these parameters are not used in subsequent case examples but are chosen to most cleanly illustrate radial drift). Solid surface densities are interpolated over raw simulation results (step-like curves). For these model parameters, the surface density at a fixed location—say $a = 1 \text{ AU}$ —rises with time in a “particle pile-up” before the entire solid disc sweeps by.

or impact parameter) is larger than the vertical thickness of the disc of solids,

$$H_s = H \sqrt{\frac{\alpha}{\alpha + \tau}} \quad (11)$$

(Youdin & Lithwick 2007), then the particles effectively comprise a 2D sheet; otherwise, the thickening of the particle layer due to turbulence reduces the pebble accretion rate by a factor R_{acc}/H_s .

OK10 identify three regimes—settling, three-body, and hyperbolic—each having their own forms for R_{acc} and v_{acc} . These formulae, modified for gas turbulence, are provided in the subsections below.

We erect local Cartesian axes centred on the core at orbital radius a , where x increases radially outward and y

advances in the direction of the core’s (assumed circular) orbital motion. Relative to the core, the particles have mean velocity (cf. equation 6)

$$v_x = -\frac{2v_{\text{hw}}\tau}{1+\tau^2} - \frac{3\nu}{2a} \frac{1}{1+\tau^2} - \dot{a}, \quad (12a)$$

$$v_y = -\frac{v_{\text{hw}}}{1+\tau^2} + \frac{3\nu}{2a} \frac{\tau}{2(1+\tau^2)} - \frac{3}{2}\Omega x \quad (12b)$$

where the terms involving τ are due to drag in sub-Keplerian, viscously accreting gas (generalizations of equations 13 and 14 of Chiang & Youdin 2010), \dot{a} is the core’s radial migration velocity (section 2.8), and the term proportional to x is from Keplerian shear. In addition to this mean relative velocity, gas turbulence imparts randomly oriented velocities to the particles of magnitude

$$v_{\text{turb}} = c_s \sqrt{\frac{\alpha}{1+\tau}} \quad (13)$$

(see Youdin & Lithwick 2007, their equation 13). The total relative speed between the core and the particles is calculated by adding in quadrature the mean $\sqrt{v_x^2 + v_y^2}$ and the fluctuation v_{turb} .

2.3.1 Settling Regime

In the settling regime, particles are well-coupled to the gas ($\tau \leq 1$). A particle is assumed to accrete onto the core if, upon approaching the core with velocity v_{acc} and acquiring a specific impulse (“kick”) Δv after the encounter, its trajectory is deflected by an order-unity angle. OK10 write this condition as $\Delta v \sim v_{\text{acc}}/4$.

For simplicity we use an expression for v_{acc} valid in the limit $\tau \ll 1$, dropping mean velocities that are typically smaller than the azimuthal headwind velocity (cf. equations 12 and 13):

$$v_{\text{acc}} \sim \sqrt{\left(v_{\text{hw}} + \frac{3}{2}\Omega R_{\text{acc}}\right)^2 + \alpha c_s^2}. \quad (14)$$

The settling regime is further defined by the condition that the particle stopping time be shorter than the encounter time:

$$\tau/\Omega < R_{\text{acc}}/v_{\text{acc}}. \quad (15)$$

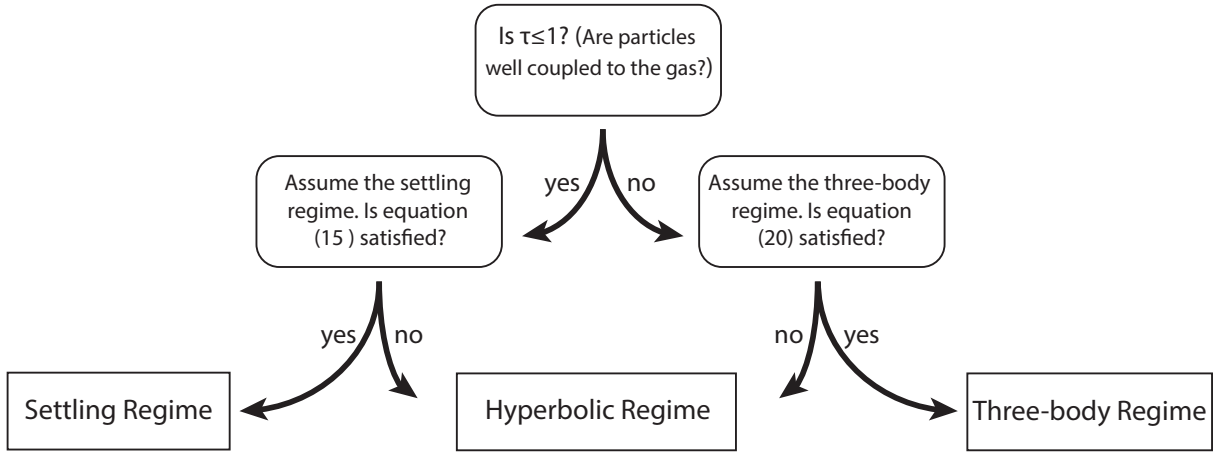


Figure 3. Flowchart for choosing the appropriate pebble accretion regime. In the case where the hyperbolic regime is returned, we perform additional *a posteriori* checks given by equations (22) and (23). In practice, for our parameters, pebble accretion is nearly always in the settling regime.

Under this assumption, the kick velocity is

$$\Delta v \sim \frac{GM_{\text{core}}}{R_{\text{acc}}^2} \frac{\tau}{\Omega}, \quad (16)$$

i.e., the particle is assumed to attain terminal velocity during the encounter (with the gravitational force from the core balancing gas drag). Setting Δv equal to $v_{\text{acc}}/4$, and re-writing in Hill's units, we have

$$\frac{9}{4}b^6 + 3\zeta b^5 + (\zeta^2 + \alpha f_P^{-1} \mu^{-1/3} \zeta) b^4 - 144\tau^2 = 0 \quad (17)$$

which we solve for $b = R_{\text{acc}}/R_{\text{Hill}}$. Here $R_{\text{Hill}} = \mu^{1/3} a$, $\mu = M_{\text{core}}/(3M_*)$, M_* is the stellar mass, $\zeta = v_{\text{hw}}/v_{\text{Hill}}$, $v_{\text{Hill}} = \Omega R_{\text{Hill}}$, and $f_P = -(1/2)\partial \log P_g / \partial \log a$. Having solved (17) for R_{acc} , we insert into (14) to evaluate v_{acc} . Our equation (17) is analogous to equation (27) of OK10 except that our accounting for turbulence in v_{acc} has resulted in a higher-order polynomial.

2.3.2 Three-Body Regime

In the three-body regime, particles execute trajectories in and around the Hill sphere that are perturbed only slightly by gas drag ($\tau \gg 1$). Accretion in this regime should be similar to that of a sub-Hill disc and its chaotic Hill sphere dynamics (Goldreich et al. 2004, their sections 3.3 and 3.4; our 2D/3D correction factor $\min(1, R_{\text{acc}}/H_s)$ in equation 10 distinguishes between their ‘‘not very thin’’ and ‘‘very thin’’ discs). Following OK10, we take

$$v_{\text{acc}} = 3.2v_{\text{Hill}} \quad (18)$$

and

$$b = 1.7\alpha_{\text{core}}^{1/2} + \frac{1}{\tau} \quad (19)$$

where $\alpha_{\text{core}} \equiv R_{\text{core}}/R_{\text{Hill}}$ (not to be confused with the gas turbulent Mach number α), and the term $1/\tau$ is OK10's

empirical correction for how gas drag enhances the accretion cross section.

In the quasi-Hill sphere dynamics assumed by the three-body regime, the dominant velocity with which a particle approaches the core is set by the Kepler shear term $(3/2)\Omega x \sim \Omega R_{\text{Hill}} = v_{\text{Hill}}$ in equations (12)–(13). We write this defining condition as follows, assuming for simplicity that $\tau \gg 1$, and dropping the terms proportional to the viscous gas velocity $3\nu/(2a)$ and the migration velocity \dot{a} which are typically negligible compared to v_{Hill} :

$$\sqrt{4v_{\text{hw}}^2/\tau^2 + \alpha c_s^2/\tau} < v_{\text{Hill}} \quad (20)$$

which re-written in Hill's units reads

$$\tau^2 - \alpha f_P^{-1} \mu^{-1/3} \zeta \tau - \zeta^2 > 0. \quad (21)$$

When $\alpha = 0$, this reduces to the same condition $\tau \gtrsim \zeta$ used by OK10 to demarcate the three-body regime (see their Figure 7).

2.3.3 Hyperbolic Regime

In the hyperbolic regime, particle-core encounters are fast—faster than the particle stopping time:

$$R_{\text{acc}}/v_{\text{acc}} < \tau/\Omega \quad (22)$$

in violation of the settling condition (15), and also faster than the time to cross the Hill sphere at the Hill velocity:

$$R_{\text{acc}}/v_{\text{acc}} < R_{\text{Hill}}/v_{\text{Hill}} = 1/\Omega \quad (23)$$

in violation of the Hill sphere dynamics assumed by the three-body regime. The encounter therefore unfolds in a classic two-body fashion with a gravitationally focused accretion

cross section of

$$\begin{aligned} b &= \alpha_{\text{core}} \sqrt{1 + \left(\frac{v_{\text{esc}}}{v_{\text{acc}}}\right)^2} \\ &= \alpha_{\text{core}} \sqrt{1 + \frac{6}{\alpha_{\text{core}}(v_{\text{acc}}/v_{\text{Hill}})^2}} \end{aligned} \quad (24)$$

where v_{esc} is the escape velocity from the core surface and $v_{\text{esc}}/v_{\text{Hill}} = \sqrt{6}/\alpha_{\text{core}}$. In general, the relative velocity v_{acc} equals $\sqrt{v_x^2 + v_y^2 + v_{\text{turb}}^2}$; but in evaluating (12b) for v_y , we may drop the Kepler shear term since $b \ll 1$ and $\zeta = v_{\text{hw}}/v_{\text{Hill}} > 1$ in the hyperbolic regime. Thus

$$\begin{aligned} \frac{v_{\text{acc}}}{v_{\text{Hill}}} &\sim \left[\left(\frac{2\zeta\tau}{1+\tau^2} + \frac{3}{2} \frac{\alpha\zeta f_P^{-1}}{1+\tau^2} + \frac{\dot{a}}{v_{\text{Hill}}} \right)^2 \right. \\ &\quad \left. + \left(\frac{\zeta}{(1+\tau^2)} - \frac{3}{2} \frac{\alpha\zeta f_P^{-1}\tau}{2(1+\tau^2)} \right)^2 + \frac{\alpha\zeta\mu^{-1/3}}{f_P(1+\tau)} \right]^{1/2}. \end{aligned} \quad (25)$$

This matches equation (29) of OK10 when $\alpha = 0$ and $\dot{a} = 0$.

We summarize in Figure 3 our decision tree for choosing the appropriate regime of pebble accretion as we track the growth of a core. When the hyperbolic regime is selected, we verify *a posteriori* that the inequalities (22) and (23) are satisfied. In practice, we find for our model parameters that pebble accretion is almost always in the settling regime. As noted in section 2.2, in evaluating Σ_s in the accretion rate (10), we interpolate using cubic splines in the vicinity of the core.

2.4 Opening a Gap in the Gas Disc

A core exerts Lindblad torques on the gas disc that open an annular gap about its orbit. The gas surface density at the position of the planet, $\Sigma_{\text{g,planet}}$, is related to the local unperturbed value Σ_{g} by

$$\frac{\Sigma_{\text{g}}}{\Sigma_{\text{g,planet}}} - 1 = 0.043 \left(\frac{M_{\text{planet}}}{M_{\star}} \right)^2 \left(\frac{H}{a} \right)^{-5} \alpha^{-1} \quad (26)$$

(Dong & Fung 2017; see also Kanagawa et al. 2015 and Fung et al. 2014). Here $M_{\text{planet}} = M_{\text{core}} + M_{\text{gas}}$ is the total planet mass, including not only the rocky core but also any gas envelope it carries (accretion of gas onto the core is treated in section 2.6), while $M_{\star} = M_{\odot}$ is the host star mass.

Depressing the gas surface density at the position of the planet has two effects. First, it reduces—very slightly—the rate at which the solid core accretes a gas envelope (see the weak dependence on $\Sigma_{\text{g,planet}}$ in equation 28). Second and more significantly, once the gas gap becomes deep enough, orbital migration of the planet is expected to slow from Type I to Type II (section 2.8).

2.5 Halting Pebble Accretion

As a planet grows in mass and opens a deeper gap in the gas disc, local pressure gradients near gap edges may trap particles there. Lambrechts & Johansen (2014, LJ14) term the core mass above which solids can no longer drift onto the core the “pebble isolation mass.” In hydrodynamics simulations, the pebble isolation mass is found to scale as the

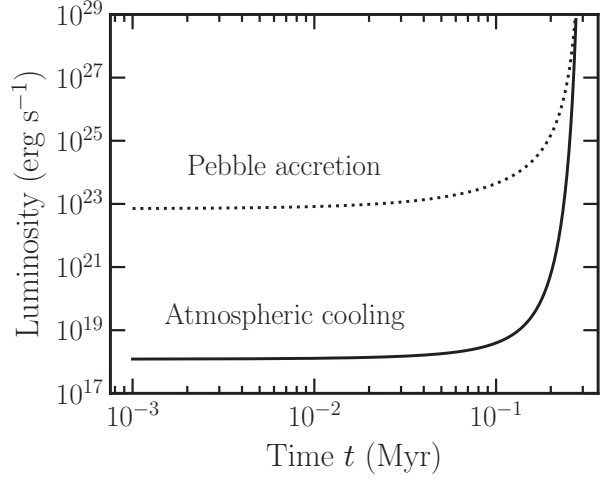


Figure 4. Pebble accretion luminosities tend to overwhelm atmospheric cooling luminosities, preventing gas from accreting onto solid cores until after pebbles have stopped accreting. The pebble accretion luminosity (dotted curve) is computed as $G M_{\text{core}} \dot{M}_{\text{core}} / R_{\text{core}}$, where \dot{M}_{core} is computed using (10) and R_{core} derives from M_{core} assuming a fixed bulk density of 5 g cm^{-3} . The core mass is initially set to $0.01 M_{\oplus}$ at a time of 10^{-3} Myr, and accretes pebbles with size $s = 0.1 \text{ cm}$ at a nearly constant $a = 1 \text{ AU}$, in a disc for which $\alpha = 10^{-4}$, $a_1 = 100 \text{ AU}$, and the initial gas and solid masses are $M_{\text{disc,g}}(0) = 10 M_J$ and $M_{\text{disc,s}}(0) = 100 M_{\oplus}$ (these same disc parameters are adopted for Figure 8). The core grows until the solid disc drifts entirely inside of the core’s orbit, at which point $M_{\text{core}} \simeq 3 M_{\oplus}$. To compute the atmospheric cooling luminosity (solid curve), we use Lee & Chiang (2015, their equations 8 and afterward), with T_{rec} set equal to 260 K, opacity constants appropriate to their section 2.2.2 for dust-free and gas-rich discs, and the gas-to-core mass ratio fixed at GCR = 0.01; assuming a higher GCR only lowers the cooling luminosity and strengthens the point of this plot.

thermal mass (that for which surface density perturbations excited by the planet become non-linear):

$$M_{\text{peb,iso}} = 5M_{\oplus} \left(\frac{H/a}{0.03} \right)^3 \left[0.34 \left(\frac{-3}{\log_{10} \alpha} \right)^4 + 0.66 \right] \quad (27)$$

(Bitsch et al. 2018; see also equations 33 and 36 of Dipierro & Laibe 2017; Rosotti et al. 2016; LJ14).

In our model, a core stops accreting particles either when (a) $M_{\text{planet}} > M_{\text{peb,iso}}$, or (b) the entire disc of solids has drifted past the core (section 2.2). Outcome (b) will prove common.

2.6 Gas Accretion onto Cores

Cores accrete as much gas as can cool—which it cannot while pebble accretion is ongoing, as the rate of accretional heating tends to exceed the rate of envelope cooling by orders of magnitude (Figure 4). We therefore start gas accretion onto solid cores only after the cores have finished accreting pebbles (section 2.5).

We adopt the scaling relation for atmospheric growth derived by Lee & Chiang (2015, their equation 24, derived for temperatures between 100 K and 800 K), accounting

for the weak dependence on nebular surface density (Lee & Chiang 2016, their Figure 4; we have verified that this density dependence applies at different distances):

$$\frac{M_{\text{gas}}}{M_{\text{core}}} = 0.20 \left(\frac{\Delta t}{0.1 \text{ Myr}} \right)^{0.4} \left(\frac{500 \text{ K}}{T} \right)^{1.5} \times \left(\frac{M_{\text{core}}}{5 M_{\oplus}} \right)^1 \left(\frac{\Sigma_{g,\text{planet}}}{0.03 \Sigma_{\text{mmen}}} \right)^{0.12} \quad (28)$$

where M_{gas} is the planetary gas mass, Δt is the elapsed time since the onset of gas accretion, T is the nebular temperature, and Σ_{mmen} is the surface density of the minimum-mass extrasolar nebula (Chiang & Laughlin 2013):

$$\Sigma_{\text{mmen}} = 4 \times 10^5 \left(\frac{a}{0.1 \text{ AU}} \right)^{-1.6} \text{ g/cm}^2. \quad (29)$$

Equation (28) drops the contribution from any dust to the gas opacity; this is a plausible assumption given grain coagulation, settling, and ablation (Ormel 2014; Brouwers et al. 2018). The two equations further presume that the bulk of the envelope mass is centrally concentrated near the core, i.e., the adiabatic index $\gamma_{\text{ad}} < 4/3$ in the inner convective zone. This assumption is valid when envelope temperatures > 2500 K so that H₂ dissociates. Only cores more massive than about $0.5 M_{\oplus}$ can gravitationally retain such gas, and so we apply equation (28) to grow atmospheres only for cores which exceed $0.5 M_{\oplus}$ at the end of the pebble accretion phase.¹ For such cores, we combine the time derivatives of equation (28) with the planet's time-varying orbital distance (section 2.8) and the disc's time-varying surface density (section 2.1) to track increments in the planet's gas mass as ambient nebular conditions change. In taking the time derivative of (28), we ignore terms depending on dT/dt and $d\Sigma_{g,\text{planet}}/dt$ for simplicity. We also check that the envelope mass does not exceed the value that it would have if it were isothermal at the disc temperature; this is the maximum mass to which the atmosphere can grow, as gas cannot cool past this point (see Lee & Chiang 2015, their Figure 4). If the envelope mass exceeds this isothermal bound, we halt gas accretion.

2.7 Runaway Gas Accretion and the Formation of Jupiters

Once the gas envelope mass becomes comparable to the underlying core mass, the envelope's self-gravity becomes significant. Self-gravitating envelopes demand larger luminosities to sustain hydrostatic equilibrium; as gas continues to pile on, the cooling timescale shortens catastrophically, and the envelope grows in a runaway fashion (e.g., Pollack et al. 1996). We crudely model runaway using a step function: once $M_{\text{gas}}/M_{\text{core}} \geq 0.5$, we boost $M_{\text{planet}} = M_{\text{gas}} + M_{\text{core}}$ to $1 M_J$, or we add to M_{gas} the total mass in the gas disc outside the planet's orbit, whichever option yields a smaller M_{planet} . The latter option is not to be taken literally (i.e., we do not literally set Σ_g to zero outside the planet's orbit), but is merely a rough proxy for mass conservation.

¹ We have also determined, following the methodology of Lee et al. (2014), that core masses $< 0.5 M_{\oplus}$ take longer than ~ 10 Myrs to accrete even 1%-by-mass envelopes.

2.8 Disc-Driven Migration

We define a “deep” gap as one for which $\Sigma_{g,\text{planet}} = 1/10$ the value of the unperturbed surface density Σ_g . From (26), deep gaps are opened by planet masses exceeding

$$M_{\text{Type II}} = 14.5 M_{\star} \alpha^{1/2} \left(\frac{H}{a} \right)^{5/2} = 8 M_{\oplus} \left(\frac{\alpha}{10^{-4}} \right)^{1/2} \left(\frac{H/a}{0.03} \right)^{5/2}. \quad (30)$$

Planets for which $M_{\text{planet}} < M_{\text{Type II}}$ are transported radially according to the Type I migration rate:

$$\dot{a} = \frac{2\Gamma_{\text{tot}}}{M_{\text{planet}} \Omega a} \quad (31)$$

where Γ_{tot} is the combined Lindblad and corotation torque exerted by the disc on the planet (e.g., Kley & Nelson 2012):

$$\Gamma_{\text{tot}} \approx -2.2 \left(\frac{M_{\text{planet}}}{M_{\star}} \right)^2 \left(\frac{a}{H} \right)^2 \Sigma_{g,\text{planet}} a^4 \Omega^2. \quad (32)$$

All quantities are evaluated at the location of the planet. The numerical pre-factor is calibrated using the hydrodynamical simulations of D'Angelo & Lubow (2010) for the power-law indices describing our gas surface density and temperature profiles. For $M_{\text{planet}} > M_{\text{Type II}}$, we switch the migration rate from Type I to Type II:

$$\dot{a} = -\frac{\alpha c_s H}{a} \times \min(1, \Sigma_g a^2 / M_{\text{planet}}). \quad (33)$$

The correction factor $\min(1, \Sigma_g a^2 / M_{\text{planet}})$ accounts for how the planet adds an extra load to the disc whose viscous drift rate is then slowed (note that we assume Σ_g and not $\Sigma_{g,\text{planet}}$ is relevant for this correction). Duffell et al. (2014) point out that the actual Type II rate could differ from (33) by factors of several because disc gas can cross the gap; we neglect this effect.

2.9 Implementation Summary

There are five input parameters governing the disc: α , a_1 , s , $M_{\text{disc,g}}(0)$, and $Z \equiv M_{\text{disc,s}}(0)/M_{\text{disc,g}}(0)$. For the planet, we have another three inputs: the initial core mass $M_{\text{core}}(0)$, the initial gas mass $M_{\text{gas}}(0)$, and the initial orbital radius $a(0)$. For all simulations, we fix $M_{\text{core}}(0) = 10^{-2} M_{\oplus}$ and $M_{\text{gas}}(0) = 0$. All other parameters are systematically varied across 540 different models; see Table 1.

Equation (10), the time derivative of equation (28), and equation (31) (or equation 33 once $M_{\text{planet}} > M_{\text{Type II}}$) define a coupled system of differential equations for the time evolution of the planet's core mass, gas mass, and orbital radius. The background gas disc evolves according to (1), and the background solid disc is evolved according to the Lagrangian ring scheme described at the end of section 2.2. Each model is evolved from $t = 10^{-3}$ Myr to 100 Myr, with state variables recorded at 5000 log-spaced times. To advance from one recording time to the next, we first evolve our background solid disc using a fourth-order Runge-Kutta method, and then solve for the planet variables using SciPy's `odeint`. A core stops growing in solid mass either once it reaches the pebble isolation mass (equation 27) or the disc of solids drifts wholly interior to the core's orbit. Once the planet's gas mass reaches half its core mass, then either

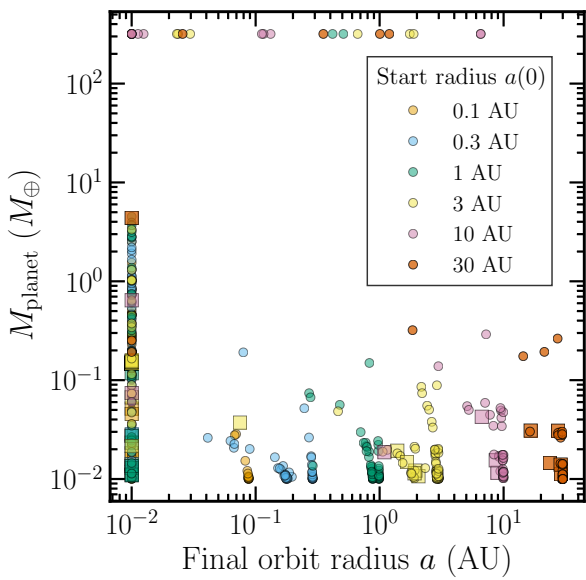


Figure 5. Final planet mass vs. final orbital distance for each of 540 parameter configurations (see Table 1). Each point is coloured according to the initial position of the seed core $a(0)$. Those models with a solid drift timescale, $a_1/[v_{\text{drift}}(a_1, 0)]$, longer than 1 Myr are marked as squares, while discs with shorter drift timescales are marked as circles. Certain parameter choices lead to cold, warm, and hot Jupiters (top line of points), all of which experience migration, and none of which materialize from long-lived solid discs (no squares, only circles). No super-Earths/sub-Neptunes form outside of the innermost disk edge at 0.01 AU; we are inclined to rule out those models where super-Earths are found at the innermost edge at $a = 0.01$ AU having migrated there, as such models would predict short-period pile-ups in super-Earth occurrence rates that are not observed (Lee & Chiang 2017). Over most of our parameter space, cores hardly grow, remaining $\lesssim 0.1 M_\oplus$.

M_{planet} is manually set to $1 M_J$, or M_{gas} is augmented by the gas disc mass outside the planet’s orbit at that time, whichever yields the smaller planet mass. Planets that migrate to our inner disc radius of $a_{\text{in}} = 0.01$ AU are held there.

3 RESULTS

Figure 5 summarizes our model outcomes. Beyond ~ 0.1 AU—in those regions where the majority of exoplanets are detected—we find that sub-Earth cores either remain sub-Earths, or explode into gas giants. There is no in-between; super-Earths are completely absent outside the assumed disc edge at 0.01 AU. Over most of the parameter space that we chart, sub-Earths are the norm: they outnumber gas giants by about 20 to 1. Moreover, these sub-Earths have hardly grown from their initial assumed seed masses of $10^{-2} M_\oplus$; on the whole, they have increased their mass by factors of several at most.

A small fraction (6%) of models produce super-Earths ($\sim 1\text{--}10 M_\oplus$). Formed overwhelmingly at short distances ($a(0) \leq 1$ AU) and/or in gas-heavy discs, the cores of

these super-Earths rapidly migrate and become stranded at the disc innermost edge, where the surrounding nebula is so hot that gas accretion onto cores is stunted—the atmospheric masses hit their isothermal upper bounds (evaluated at $T = 2600$ K at $a = 0.01$ AU). Final gas-to-core mass ratios are about 1–10%, with a few reaching up to 30%. These migration-heavy models predict that planets pile up at short orbital periods (see, e.g., Ida & Lin 2008). Because such pile-ups are not seen in observations (see, e.g., Lee & Chiang 2017, and references therein), we tend to discount as unrealistic those model parameters that lead to such wholesale migration of cores.

Whether a core nucleates a gas giant depends on its mass: more massive cores accrete gas faster (Pollack et al. 1996; Piso & Youdin 2014; Lee & Chiang 2015; Ginzburg et al. 2016). In the following, we describe analytically the factors that determine how quickly and to what final mass a core grows by pebble accretion—including how much disc mass is expended in the process. These pencil-and-paper considerations help to explain our numerical results, which are also fleshed out in greater detail below.

The final mass of the core is determined by how many pebbles the seed core nets from the background drift of solids (orbital migration of the core can be safely neglected during this early growth phase). From equation (6) for v_{drift} , the time it takes for the solid disc to drain from its initial outer radius a_1 to the location of the core a is

$$t_{\text{drift}} \simeq \begin{cases} a/(2v_{\text{hw}}\tau) \ln(a_1/a), & \tau \gg \alpha \\ (2/3)\alpha^{-1}(\Omega a/c_s^2)(a_1 - a), & \tau \ll \alpha \end{cases} \quad (34)$$

where all unsubscripted variables (here and below) are evaluated at the position of the core. We have taken the limit $\tau \ll 1$ (valid over practically all of our parameter space) and made use of the fact that for our assumed disc gas surface density and temperature profiles, $\tau \propto a$ and $v_{\text{hw}} = \text{constant}$.

Because pebble accretion for our parameters occurs mostly in the settling regime ($\tau < 1$), and with $R_{\text{acc}} < H_s$ (see Appendix A for a more general exposition; see also Ormel 2017), we can write:

$$\dot{M}_{\text{core}} = 2\Sigma_s R_{\text{acc}}^2 v_{\text{acc}}/H_s = \frac{8\Sigma_s GM_{\text{core}}\tau}{c_s} \left(\frac{\alpha + \tau}{\alpha}\right)^{1/2}. \quad (35)$$

Accordingly, the core grows exponentially with time:

$$M_{\text{core}}(t) = M_{\text{core}}(0) \exp \left[\frac{8G\tau}{c_s} \left(\frac{\alpha + \tau}{\alpha} \right)^{1/2} \int_0^t \Sigma_s dt \right] \quad (36)$$

assuming τ at the position of the core is constant with time (which it approximately is in our models at early times; see our later figures). For $\tau \gg \alpha$, we can use the relations $v_{\text{drift}} \propto v_{\text{hw}}\tau \propto a$ (Epstein) and $\Sigma_s \propto a^{-1}$ to solve the continuity equation for Σ_s by separation of variables: $\Sigma_s(a, t) = f(a)g(t) \propto a^{-1}g(t)$, whence $g(t) = \exp[t/(a/v_{\text{drift}})]$ (i.e., an exponentially rising “particle pile-up” at fixed location; see, e.g., Figure 2). Then the final core mass after $t = t_{\text{drift}}$ is

$$M_{\text{core}} \sim M_{\text{core}}(0) \exp \left[\frac{2}{\pi} \left(\frac{\tau}{\alpha} \right)^{1/2} \frac{M_{\text{disc},s}(0)}{M_*} \left(\frac{\Omega a}{c_s} \right) \left(\frac{\Omega a}{v_{\text{hw}}} \right) \right], \quad \tau \gg \alpha \quad (37)$$

where we have used $M_{\text{disc},s}(0) = 2\pi\Sigma_s(a, t = 0)a a_1$. For

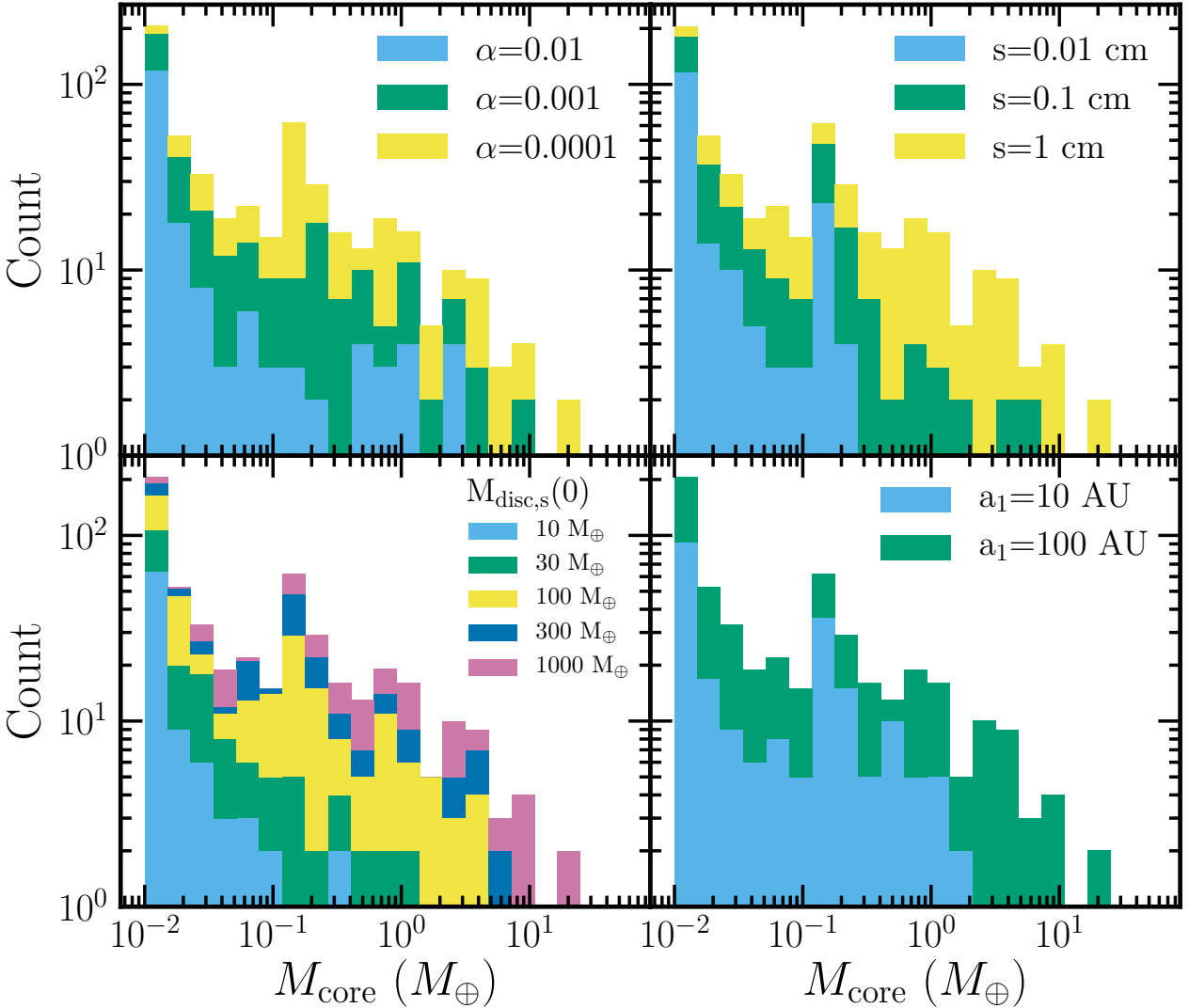


Figure 6. Final core mass histograms, stacked and coloured against various model input parameters. We see that higher mass cores prefer lower α , higher s , higher $M_{\text{disc},s}(0)$, and higher a_1 . See text for discussion.

$\tau \ll \alpha$, Σ_s is approximately constant in time (since $\Sigma_s \propto a^{-1}$ is the steady-state solution for $v_{\text{drift}} = 3\nu/(2a) = \text{constant}$), and so

$$M_{\text{core}} \sim M_{\text{core}}(0) \exp \left[\frac{8}{3\pi} \left(\frac{\tau}{\alpha} \right) \frac{M_{\text{disc},s}(0)}{M_*} \left(\frac{\Omega a}{c_s} \right)^3 \frac{a_1 - a}{a_1} \right],$$

$$\tau \ll \alpha. \quad (38)$$

From equations (37) and (38), it follows that more massive cores, and by extension Jupiters, favour high $M_{\text{disc},s}(0)$, high τ (to enable particles to more easily ‘peel off’ the gas flow and fall onto the core), and low α (to reduce the particle scale height and increase the solid particle density; and, in cases where the pebble drift speed is determined by viscosity, to slow that drift speed down and prolong the time over which the core accretes). Figure 6 verifies these dependencies, at least in sign. More massive cores are formed in discs with higher overall solid mass (lower left panel), smaller α

(upper left panel), larger pebble size s (which increases τ ; upper right panel and equation 9), and larger a_1 (which also increases τ by spreading a given gas mass over a larger area to reduce the gas density; lower right panel and equation 9).

Equations (37) and (38) further suggest that the ratio τ/α is a key parameter controlling how massive cores can grow. Figure 7 bears this out by showing that Jupiter-breeding cores only form when $\tau/\alpha > 0.1$. The condition $\tau/\alpha > 0.1$ is necessary but not sufficient to create gas giants; the vast majority of our runs at $\tau/\alpha > 0.1$ yield only sub-Earths, mostly because $M_{\text{disc},s}(0)$ is too small. Another necessary condition for spawning giants is that their cores grow outside ~ 0.1 AU—sufficiently far away from their host stars that they do not run up against the pebble isolation mass, which decreases with decreasing distance to the star ($M_{\text{peb,iso}} \propto a^{3/4}$; see equations 27 and 5). This limitation set by pebble isolation argues against in-situ formation of

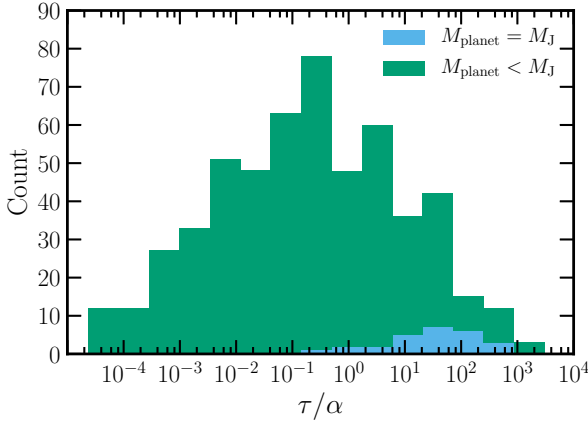


Figure 7. Histogram of the ratio τ/α for our 540 models, where Stokes number τ is evaluated at the initial time (and in practice remains constant over most if not all of the duration of core growth; see following figures). The histogram is additionally stacked and coloured according to whether or not a gas giant emerges from a given model. All gas giants arise from model parameter combinations for which $\tau/\alpha > 0.1$. This necessary condition on core growth is consistent with analytic calculations; see discussion surrounding equations (37) and (38).

hot Jupiters. An example of core growth stifled by pebble isolation will be given below.

A core accretes only a fraction of the solids from the outer disc that converge onto its orbit. The remaining fraction drifts past the core into the inner disc and is “wasted”. To grow a core from an initial seed mass $M_{\text{core}}(0)$ requires a mass investment of

$$M_{\text{drift}} = \int_{M_{\text{core}}(0)}^{M_{\text{core}}} \epsilon^{-1} dM_{\text{core}} \quad (39)$$

where the instantaneous pebble accretion efficiency

$$\epsilon \equiv \frac{\dot{M}_{\text{core}}}{2\pi\Sigma_s v_{\text{drift}} a} = \frac{4}{\pi} \left(\frac{\Omega a}{v_{\text{drift}}} \right) \left(\frac{\Omega a}{c_s} \right) \left(\frac{M_{\text{core}}}{M_*} \right) \tau \left(\frac{\alpha + \tau}{\alpha} \right)^{1/2}. \quad (40)$$

Note how ϵ , and by extension M_{drift} , do not depend on Σ_s and the details of its time evolution. Evaluation gives:

$$M_{\text{drift}} = \frac{\pi}{4} \left(\frac{v_{\text{drift}}}{\Omega a} \right) \left(\frac{c_s}{\Omega a} \right) \tau^{-1} \left(\frac{\alpha}{\alpha + \tau} \right)^{1/2} M_* \ln \left[\frac{M_{\text{core}}}{M_{\text{core}}(0)} \right] \sim \begin{cases} 35 M_\oplus \left(\frac{a}{1 \text{ AU}} \right)^{3/4} \left(\frac{10}{\tau/\alpha} \right)^{1/2} \ln \left(\frac{M_{\text{core}}/M_{\text{core}}(0)}{100} \right), & \tau \gg \alpha \\ 600 M_\oplus \left(\frac{a}{1 \text{ AU}} \right)^{3/4} \left(\frac{0.1}{\tau/\alpha} \right) \ln \left(\frac{M_{\text{core}}/M_{\text{core}}(0)}{100} \right), & \tau \ll \alpha \end{cases}. \quad (41)$$

These analytic estimates appear consistent with our numerical results as reported in Figure 6 (lower left panel).

Example evolutionary tracks of seed cores that grow to gas giants are presented in Figures 8 (warm Jupiter), 9 (cold Jupiter), and 10 (hot Jupiter). For comparison we also show simulations that terminate in sub-Earths in Figures 11, 12, and 13, illustrating three different modes by which gas giant formation by pebble accretion can fail (low $M_{\text{disc,s}}(0)$; low $M_{\text{peb,iso}}$; and $\tau/\alpha < 0.1$, respectively).

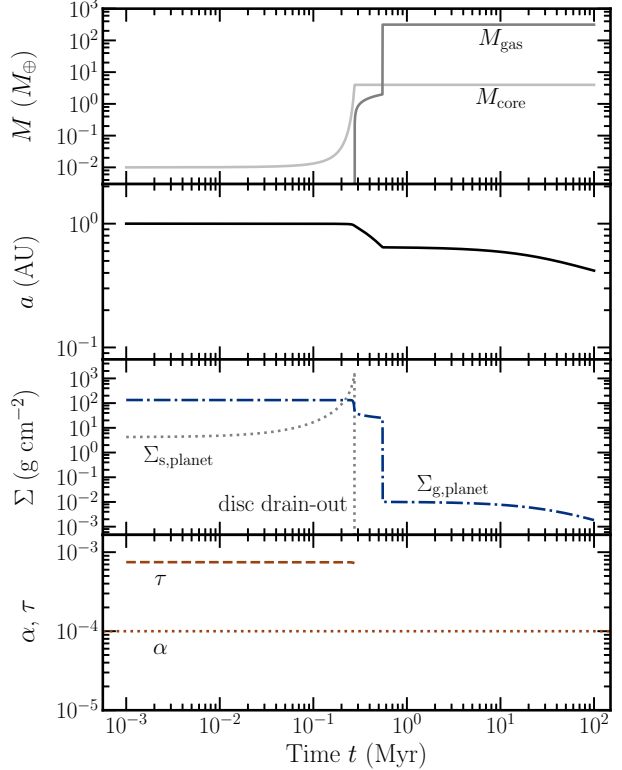


Figure 8. Genesis of a warm Jupiter. All quantities are evaluated at the location of the planet. The core mass M_{core} grows most rapidly when the local solid surface density $\Sigma_{\text{s},\text{planet}}$ rises from a particle pile-up (compare first and third panels from the top). This pile-up just precedes the drain-out of solids from outside the core’s orbit (see, e.g., Figure 2). Dips in $\Sigma_{\text{g},\text{planet}}$ reflect the deepening of gaps in the gas disc following planet mass growth. According to our toy prescription for runaway gas accretion, when the planet’s gas mass $M_{\text{gas}} = 0.5M_{\text{core}}$, we instantly set the total planet mass $M_{\text{planet}} = M_{\text{gas}} + M_{\text{core}} = 1M_J$. The planet has technically not stopped migrating at the end of the simulation, but we expect it to eventually park not too far away, given the steady decline in $\Sigma_{\text{g},\text{planet}}$ from viscous diffusion onto the star (the actual migration history will depend on the actual dispersal history of the disc which is beyond the scope of this paper). Input parameters for the model shown are: $\alpha = 10^{-4}$, $s = 0.1$ cm, $a_1 = 100$ AU, $a(0) = 1$ AU, $M_{\text{disc,g}} = 10 M_J$, $M_{\text{disc,s}} = 100 M_\oplus$.

For all evolutionary tracks, we verify that the core mass grows at least exponentially fast. Note how in those runs for which $\tau > \alpha$ (Figures 8–12), the solid surface density Σ_s at the location of the core rises with time just before the solid disc drifts entirely past the core. This “particle pile-up”—a traffic jam in disc solids—occurs whenever the particle drift velocity v_{drift} decreases sufficiently fast with decreasing radius (Youdin & Chiang 2004). We have verified that such an inwardly decreasing velocity profile obtains when $\tau/\alpha > 0.1$ —so that the drift velocity in (6) is not dominated by viscous diffusion but has a significant contribution from aerodynamic drag—and when that drag is in the Epstein regime for $\tau \ll 1$. The latter drag regime typically holds between ~ 0.1 and ~ 10 AU for our model parameters; outside ~ 10 AU, τ approaches unity and the velocity profile flattens, while inside ~ 0.1 AU, Stokes drag obtains which

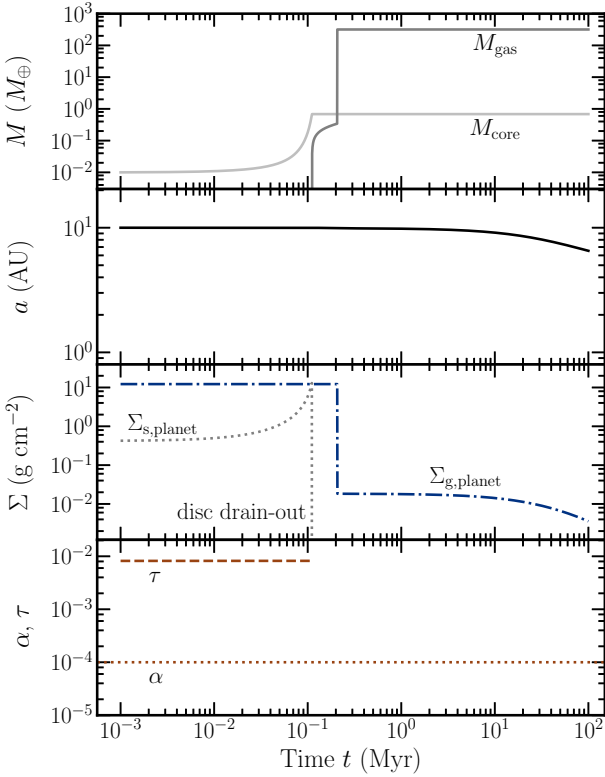


Figure 9. Genesis of a cold Jupiter. Caption text for Figure 8 applies here. Input parameters: $\alpha = 10^{-4}$, $s = 0.1$ cm, $a_1 = 100$ AU, $a(0) = 10$ AU, $M_{\text{disc,g}} = 10 M_J$, $M_{\text{disc,s}} = 100 M_\oplus$.

bleeds particles from the inside out. Where there is a particle pile-up, core growth is super-exponentially fast (equation 36).

Although we have identified model parameters that succeed in forming Jupiters by pebble accretion, these same parameters encounter difficulty when confronted with millimetre-wavelength observations of discs. The problem is that rapid core growth by pebble accretion demands large τ (equations 37 and 38), but that same large τ leads to solids draining quickly from the disc (equation 34)—too quickly when compared against observations. In all of our Jupiter-forming runs, solids drain out in ~ 0.1 – 0.3 Myr (Figures 5 and 8–10) or shorter (data not shown). These results cannot be immediately reconciled with observed discs that orbit stars 1–10 Myr old and that exhibit mm-wave continuum emission—presumably from mm-sized solids—on scales of 10–100 AU (e.g., Tripathi et al. 2017; Tazzari et al. 2016; Pérez et al. 2015).

4 SUMMARY AND DISCUSSION

We have studied how planets can form by pebble accretion, starting from an assumed seed mass of $10^{-2} M_\oplus$ and working our way to cores massive enough to nucleate gas giants. Our model is global in the sense that it accounts for the parent disc over its entire radial extent. We calculated how solids drift from large to small orbital radius by aerodynamic drag

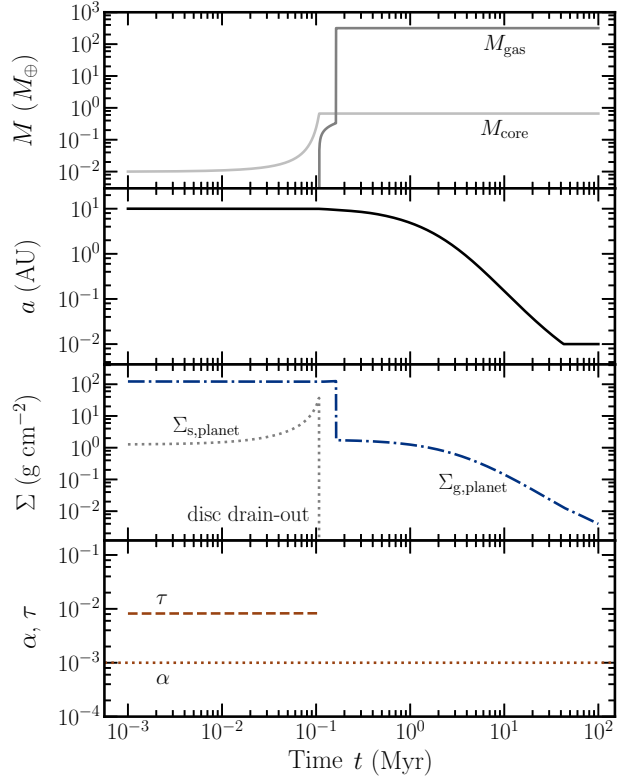


Figure 10. Genesis of a hot Jupiter. Caption text for Figure 8 applies here. Input parameters: $\alpha = 10^{-3}$, $s = 1$ cm, $a_1 = 100$ AU, $a(0) = 10$ AU, $M_{\text{disc,g}} = 100 M_J$, $M_{\text{disc,s}} = 300 M_\oplus$.

within viscously spreading gas, and how the disc has only a finite reservoir of solids with which to build planets. A fixed pebble size of 0.01–1 cm was assumed. Prescriptions for pebble accretion were taken from Ormel & Klahr (2010) and modified for gas turbulence, while those for gas accretion onto cores were drawn from Lee & Chiang (2015, 2016).

We summarize our results as follows, placing them into context with observations:

(i) *Growth by pebble accretion is exponentially sensitive to solid disc mass.* The solid disc mass controls not only how massive a core can grow, but also how fast it grows. That growth is at least exponentially fast during the earliest stages if not the entire duration of pebble accretion, with an e-folding time that scales inversely with the disc solid surface density. Growth can be super-exponentially fast if outer disc solids “pile up” at the position of the core as they drift inward.

This strong sensitivity of core growth to disc solid content, coupled with the need for Jupiters to nucleate from sufficiently massive cores, accords with the observation that the occurrence rates of gas giants (Fischer & Valenti 2005) and of larger planets more generally (Buchhave et al. 2014; Petigura et al. 2018) correlate with host star metallicity (to the extent that the latter can be used as a proxy for solid disc content). Although the expectation that discs with more solids spawn more massive cores may seem obvious, and is not specific to pebble accretion but also characterizes core

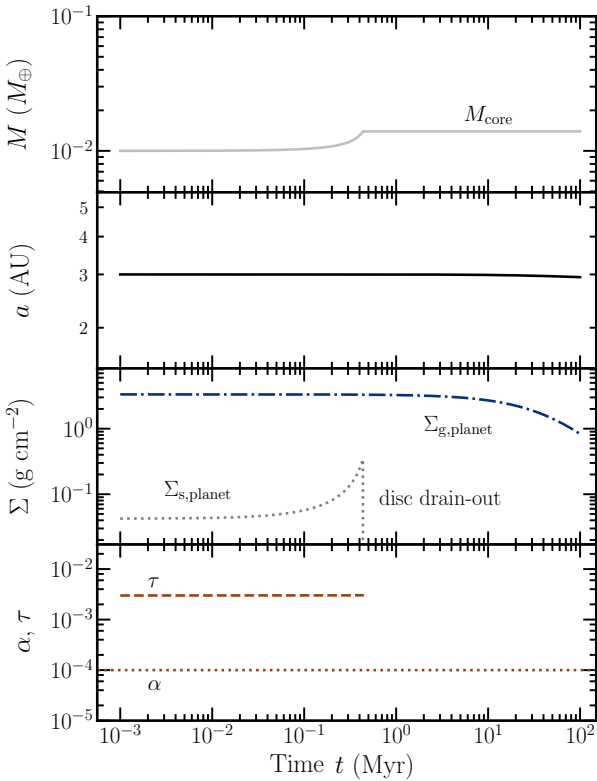


Figure 11. A case where pebble accretion fails to grow much of anything. Although $\tau > \alpha$ (see Figure 7), the total inventory of solids $M_{\text{disc,s}}$ is too small. Plot format follows that of Figure 8. Input parameters: $\alpha = 10^{-4}$, $s = 0.01$ cm, $a_1 = 100$ AU, $a(0) = 30$ AU, $M_{\text{disc,g}} = 10 M_J$, $M_{\text{disc,s}} = 30 M_\oplus$.

formation by giant impacts (Dawson et al. 2015), it is not a universal prediction of theory—not even in the context of pebble accretion. For example, if the final core mass were limited instead by the pebble isolation mass (e.g., Lambrechts et al. 2014), a correlation between planet radius and host star metallicity would not be expected, as the pebble isolation mass has no dependence on disc solid mass (see equation 27). In our simulations, pebble isolation is not an issue unless the core migrates inside ~ 0.1 AU; what typically limits the core mass instead is the fact that the disc only has so much mass to give before it drifts past the core.

(ii) *Pebble accretion depends sensitively on particle size and turbulent vertical stirring, and loses orders of magnitude more mass to radial drift than is actually used to build cores.* Forming cores massive enough to nucleate gas giants (i.e., Earth-mass or larger objects) places stringent constraints on the parent disc. Not only must the disc contain enough solids ($M_{\text{disc,s}} > 30 M_\oplus$), but those solids should have aerodynamic stopping times not too short, and be embedded in gas that is not too turbulent. More quantitatively, over much of our parameter space, the final core mass increases exponentially with τ/α raised to some power (equations 37 and 38), with $\tau \equiv \Omega_{\text{stop}} < 1$ the dimensionless measure of particle stopping time, Ω the orbital angular frequency, and $\alpha < 1$ the turbulent Mach number. As τ increases up to unity, the accretion cross-section of the core grows; as α de-

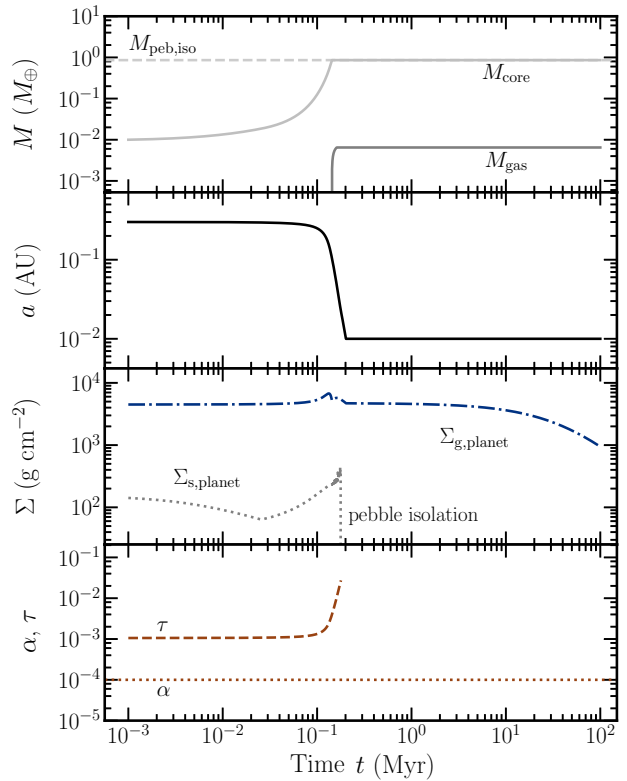


Figure 12. A case where pebble accretion forms a hot Earth but not a Jupiter. Although $\tau > \alpha$ and $M_{\text{disc,s}}$ is assigned its highest possible value, a gas giant fails to form because the planet's orbital radius starts small and only gets smaller by migration. Small orbits are more susceptible to pebble isolation ($M_{\text{peb,iso}} \propto a^{3/4}$; see equations 27 and 5), which is what ultimately limits the core mass here. Gas accretion is quickly terminated once the atmospheric mass reaches the upper bound appropriate to an isothermal atmosphere—an upper bound made low by the high temperature (2600 K) at the innermost disk edge. Plot format follows that of Figure 8. Input parameters: $\alpha = 10^{-4}$, $s = 1$ cm, $a_1 = 100$ AU, $a(0) = 0.3$ AU, $M_{\text{disc,g}} = 100 M_J$, $M_{\text{disc,s}} = 1000 M_\oplus$.

creases, the vertical thickness of the solid disc decreases and the density of accreting particles increases. We find empirically that Jupiter-breeding cores require $\tau/\alpha > 0.1$. Even when this condition is satisfied, pebble accretion is wasteful in the sense that $\gtrsim 97\%$ of the solids can be lost to radial drift while growing a core from a lunar mass to a few Earth masses.

(iii) *Sub-Earths and gas giants, but no super-Earths—at least none that avoid wholesale migration to the innermost disk edge.* Pebble accretion seems to be an all-or-nothing (and usually nothing) prospect: either sub-Earth cores remain sub-Earth, growing by less than a factor of 10 in mass, or conditions are tuned such that cores grow rapidly while the disc is still gas-rich, leading to Jupiters. The exponential dependence of core mass on disc properties (equation 36) acts effectively as an on/off switch. When the switch is on, and cores grow to maximum, typically super-Earth size, they do not remain super-Earths, but run away to become

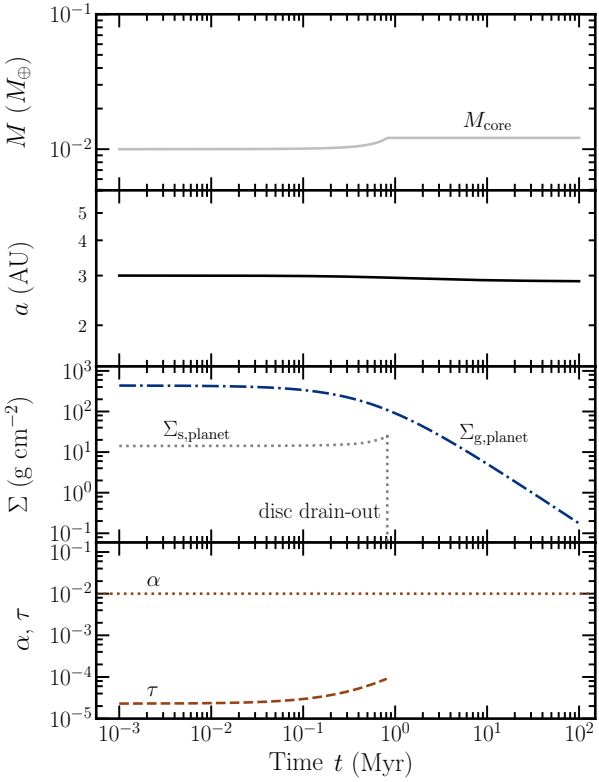


Figure 13. A case where pebble accretion is rendered practically impotent, here because $\tau \ll \alpha$; particles are too strongly coupled to gas to drop out onto cores, and particle densities are made too dilute by turbulent stirring. Furthermore, because $\tau \ll \alpha$, the particle pile-up at the planet’s position is more muted than in other figures in this series. Plot format follows that of Figure 8. Input parameters: $\alpha = 10^{-2}$, $s = 0.01$ cm, $a_1 = 100$ AU, $a(0) = 3$ AU, $M_{\text{disc,g}} = 100 M_J$, $M_{\text{disc,s}} = 1000 M_\oplus$.

Jupiters under the early-stage, gas-rich conditions presumed by pebble accretion.

Runaway can be avoided at ultra-small orbital distances where temperatures are high enough to stop gas accretion. Those few super-Earths ($1-10 M_\oplus$) that do form in our models are all located at the innermost disk edge (0.01 AU), having migrated and piled up there. The problem is that short-period pile-ups of planets are not observed (Lee & Chiang 2017); nor is it clear how to disrupt enough mean-motion resonant chains that may result from such wholesale migration (Izidoro et al. 2017; but see also Goldreich & Schlichting 2014). Super-Earths are more naturally created later in a disc’s life, under gas-poor conditions where migration is not a concern, in a series of late-stage giant impacts (e.g., Lee et al. 2014; Dawson et al. 2015, 2016; Lee & Chiang 2016; Ogihara et al. 2018).

The gas giants that form by pebble accretion also generally undergo orbital migration. This is just a simple consequence of the gas-rich conditions typically assumed by pebble accretion. The extent of migration exhibited by our model Jupiters ranges from shrinking the orbital radius by $\sim 30\%$, to complete collapse from 10 AU to the innermost disk edge—and everything in between. Contrary to the spec-

ulation that hot Jupiter cores can form in situ by pebble accretion (Batygin et al. 2016), we find that pebble isolation inside ~ 0.1 AU limits core masses to values too low to trigger runaway gas accretion within the gas disc lifetime.

(iv) *Jupiters can form by pebble accretion, but in discs that may not fit mm-wave observations.* Pebble accretion favours particles large enough to have long stopping times τ (up to unity). The problem is that such particles are also the fastest to drain out of the disc. In nearly all of our Jupiter-producing runs, the disc is emptied of 0.01–1 cm sized pebbles on timescales ranging from 0.01–1 Myr. These drift times are troublingly shorter than the 1–10 Myr ages of discs seen in thermal mm-wave emission on scales of 10–100 AU.

Our findings, in particular our conclusions about the extreme sensitivity of pebble accretion rates to disc parameters, differ somewhat from those in past studies. The differences are qualitative insofar as we are highlighting previously unappreciated difficulties in forming gas giants—and the apparent impossibility of forming super-Earths outside the innermost disc edge—by pebble accretion. For example, Lambrechts & Johansen (2014, LJ14) reported that cores with initial masses of $10^{-3} M_\oplus$ readily grow by pebble accretion to $1-10 M_\oplus$ within 1 Myr at orbital distances of 5–20 AU. See their Figure 3, which we have reproduced in our Figure 14 (dashed lines). Their result follows from their assumption that pebble accretion proceeds in the settling limit ($\tau \lesssim 1$) under two conditions: (a) the pebbles effectively comprise a 2D ultra-dense sheet whose scale height H_s is less than the accretion impact parameter R_{acc} , and (b) Keplerian shear dominates the headwind in setting the relative velocity between pebble and core (cf. our equation 14). Invoking both assumptions gives the largest possible growth rates, with maximal accretion cross-sections and velocities set by Hill-sphere scales (their equation 28). Unfortunately, unless conditions are extremely fine-tuned, neither assumption holds at low core masses $\lesssim 10^{-1} M_\oplus$ (and their starting mass is $10^{-3} M_\oplus$). In this work we have not imposed any assumption about the regime of accretion (see our general treatment in section 2.3 and the Appendix; see also Ormel 2017). By more carefully modelling pebble accretion at the earliest stages, we find that cores grow orders-of-magnitude more slowly than has been reported by LJ14 and like-minded studies; see Figure 14 for a direct comparison.

Note further that to ensure the comparison in Figure 14 is fair, we incorporated LJ14’s scheme for grain growth (their equations 20 and 25; see also Birnstiel et al. 2012). Their model disc is characterized by particle stopping times $\tau \sim 0.01-0.1$ (their Figure 1); these are relatively high values that on the one hand promote pebble accretion, but on the other lead to fast radial drift and therefore disc sizes too compact compared to mm-continuum observations. Figure 15 shows that the LJ14 model of grain growth + drift (solid lines) does not yield enough mm-cm objects at 20–60 AU to match the size-wavelength relation exhibited by TW Hya, a 3–10 Myr system. Our models suffer from the same problem, as we have noted under (iv) above.

Powell et al. (2017) solved the problem of reproducing the size-wavelength relation of TW Hya by enhancing the disc’s gas mass and slowing drift. This seems to us an acceptable solution. Our comment would be that such a disc

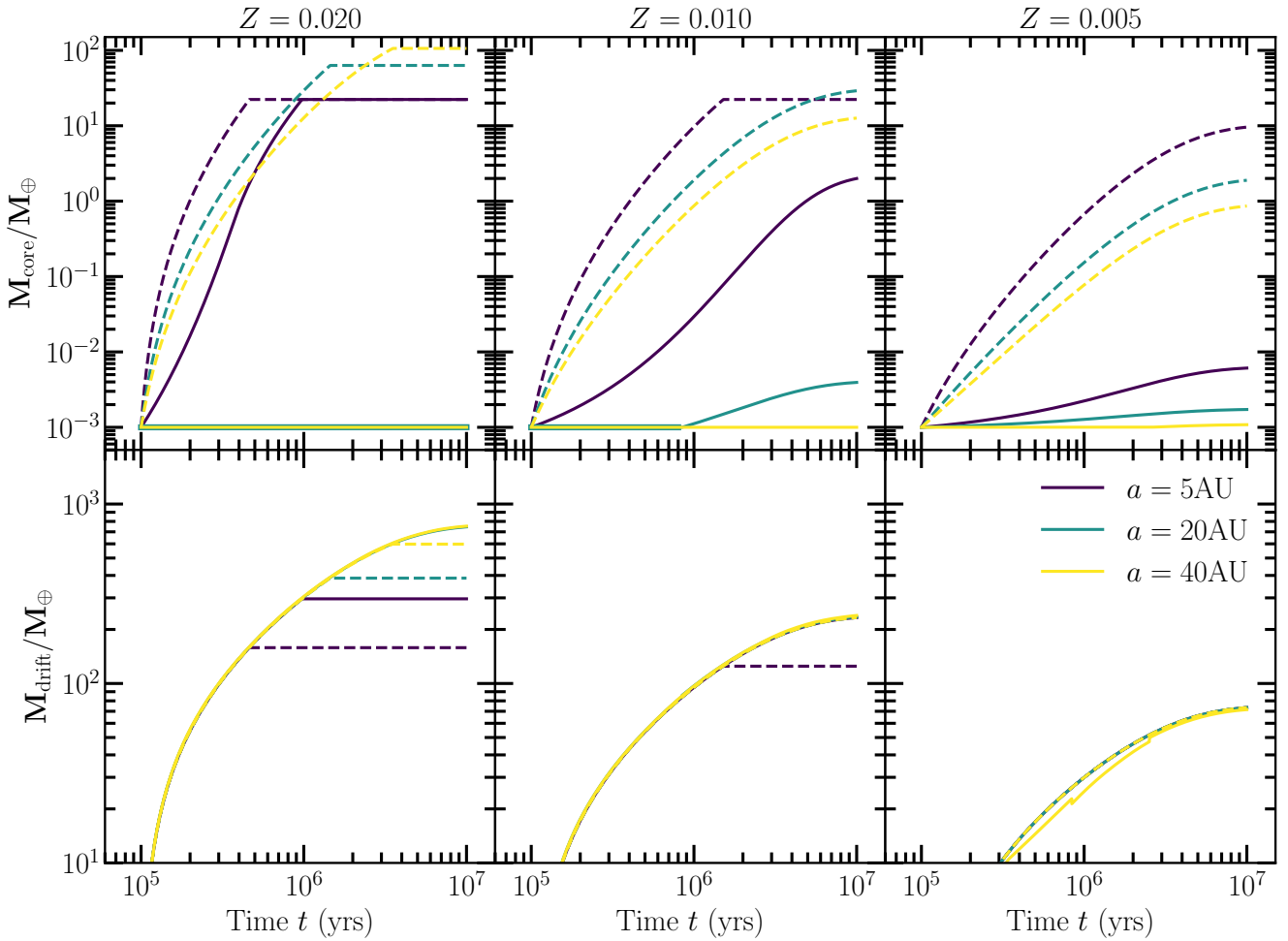


Figure 14. Comparison between the pebble accretion model of Lambrechts & Johansen (2014, LJ14) and our model. To make the comparison fair, we use the same input parameters as LJ14—in particular, we incorporate their grain growth prescriptions, as outlined in section 2 of LJ14 (their equations 20 and 25); their initial core mass of $10^{-3}M_{\oplus}$; and their fiducial gas surface density $\Sigma_g = 500 \text{ g cm}^{-2}(a/\text{AU})^{-1} \exp(-t/3 \text{ Myr})$. The only difference between their model (dashed lines) and our model (solid lines) is that they assume shear-dominated, two-dimensional ($R_{\text{acc}} > H_s$) accretion whereas we make no assumption about the regime of accretion and follow the general scheme outlined in our section 2.3. *Top:* Core mass vs. time. Core growth is truncated once the pebble isolation mass is reached (equation 27; Bitsch et al. 2018). The assumption of shear-dominated, two-dimensional accretion is seen to overestimate core growth rates by orders of magnitude. Note how at distances of 20–40 AU, cores hardly grow, especially for a disk-integrated, initial solid-to-gas mass ratio $Z (= Z_0$ in the notation of LJ14) of 0.02. In the grain growth model of LJ14, the higher is Z , the more rapidly particles grow, and the larger is τ ; for $Z = 0.02$, the stopping time is longer than the core-particle encounter time at $a = 20$ –40 AU, and pebble accretion is in the (slow) hyperbolic regime. *Bottom:* The cumulative “wasted” mass that drifts past the core as the core is still growing. All model curves necessarily overlap except when the core in a given model stops growing. Comparing the solid curves (our model) in the top panel with the solid curves in the bottom panel, we infer net pebble accretion efficiencies that are at most $M_{\text{core}}/M_{\text{drift}} \simeq 1/15$ ($Z = 0.02$, $a = 5$ AU) and for other cases much lower.

would not be conducive to pebble accretion of mm–cm sized particles whose τ ’s would be too small to accrete onto cores efficiently. Perhaps cores grow instead from super-cm (larger τ) particles that are less visible to mm continuum observations. Another way to explain the size-wavelength correlation is to invoke optically thick substructures in the inner disc; these could take the form of concentric rings of particles trapped in gas pressure maxima (see Tripathi et al. 2018 for a specific discussion of UZ Tau, and also our section 4.1 below).

Our conclusions do not seem particularly sensitive to our assumption of a single seed core. Were we to distribute seed cores over a wide range of orbital distances, those close

in would grow more-or-less independently of those far out, since any given core diverts only a small fraction—a few percent at most—of the background disc flow toward its own growth. If seed cores were packed so closely as to be competing for the same solids, and if $R_{\text{acc}} < H_s$, then growth would be “neutral” (section 8 of Goldreich et al. 2004): the distribution of relative core masses would not change, since the doubling time $M_{\text{core}}/\dot{M}_{\text{core}} \propto M_{\text{core}}^0$ (equation 35). If $R_{\text{acc}} > H_s$, then growth would be “orderly”: $M_{\text{core}}/\dot{M}_{\text{core}}$ would increase with increasing M_{core} (equations A6 and A8), and the distribution of relative core masses would narrow (Kretke & Levison 2014). In either case, spreading the mass

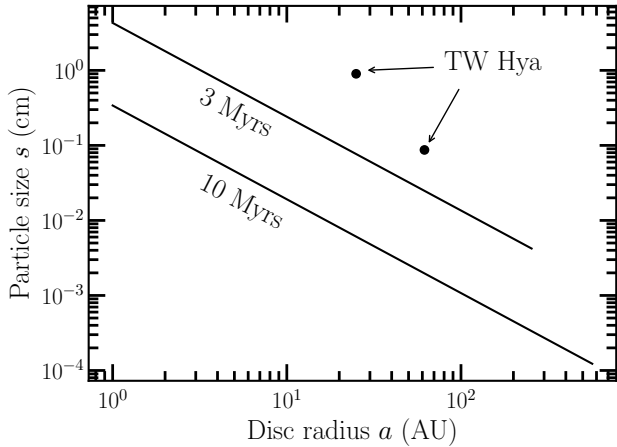


Figure 15. Comparing the grain growth model of [Lambrechts & Johansen \(2014, LJ14, solid lines\)](#) to the observed mm-cm continuum sizes of the 3–10 Myr old TW Hydra disc ([Andrews et al. 2012; Menu et al. 2014](#); black circles). The latter data are placed on this plot by assuming that the size of the emitting particles equals the wavelength of observation. The fiducial model of LJ14 predicts insufficiently large particles at 20–100 AU at an age of 3–10 Myr; by this time, mm-cm sized objects have drained out by gas drag. Staying within the framework of the LJ14 grain growth model, this discrepancy can be resolved by assuming a longer-lived gas disc (one with an e-folding time of 10 Myr), and a disk-integrated dust-to-gas ratio that is strongly supersolar ($Z = 0.1$) to enhance grain growth. An alternative (still within the context of the LJ14 model) is to make the disc so gas-heavy (approximately 10 times more massive than their fiducial disc) that it is Toomre Q -unstable ($Q \sim 0.4$ at $a = 25$ AU).

between multiple cores would only exacerbate the difficulties of growth by pebble accretion that we are calling out.

4.1 Future Directions

Our model could use improvement in many respects. There are, of course, the usual shortcomings resulting from our incomplete understanding of orbital migration (e.g., the transition from Type I to Type II); runaway gas accretion; and perhaps most glaringly, disc turbulence and transport. We focus here on issues more specific to pebble accretion.

Revisiting the gas-particle dynamics of pebble accretion from first principles seems worthwhile. Our paper is based on the equations of [Ormel & Klahr \(2010\)](#), which assume a strict Cartesian shear for the background gas disc. But cores perturb gas streamlines onto horseshoe orbits in 2D (e.g., [Ormel 2013](#), their Figure 12) and “transient horseshoes” in 3D (e.g., [Fung et al. 2015](#)), either of which can deflect particles, particularly those with small τ , away from the core, and conceivably radically altering accretion probabilities. [Xu et al. \(2017\)](#) have tested some of the scaling relations of [Ormel & Klahr \(2010\)](#) using 3D simulations, but only under restrictive conditions and with mixed results. A more comprehensive study, starting with re-deriving accretion cross sections and velocities for 2D laminar flow patterns, would be welcome (see also [Popovas et al. 2018](#)).

Images of protoplanetary discs from the Atacama Large Millimeter Array have revealed concentric rings of dust ([ALMA Partnership et al. 2015; Andrews et al. 2016; S. An-](#)

drews 2017, personal communication). These rings may trace local gas pressure maxima that can “trap” inflowing pebbles (see the review by [Pinilla & Youdin 2017](#) and references therein). Are these rings the sites of planetesimal/planet formation? How does pebble accretion proceed in the presence of traps? In particular, how would the accretion rate (35) and the efficiency (40) change if the seed core were located at the centre of the pressure bump? Because drift speeds slow to zero in traps, interparticle collisions are gentler, and bodies may stick their way to larger sizes and larger Stokes numbers (cf. [Chiang & Youdin 2010](#), their section 4), allowing for more rapid pebble accretion. How long the solids in the trap take to congeal into a single body is an outstanding question.

ACKNOWLEDGMENTS

We thank Bertram Bitsch, Wladimir Lyra, Ruth Murray-Clay, Chris Ormel, and Michael Rosenthal for helpful discussions. JWJ and EC acknowledge support from the National Science Foundation and a Berkeley BEAR grant. EJL is supported by the Sherman Fairchild Fellowship from Caltech. This research used the Savio computational cluster resource provided by the Berkeley Research Computing program at the University of California, Berkeley (supported by the UC Berkeley Chancellor, Vice Chancellor for Research, and Chief Information Officer).

APPENDIX A: REGIMES OF CORE GROWTH BY PEBBLE ACCRETION

Over much of our parameter space, the accretion radius R_{acc} is smaller than the particle scale height H_s . For a small subset of our models, at core masses above a few M_\oplus , this inequality reverses (see Figure A1; to be clear, the equations we solve are general enough to accommodate this possibility). We discuss here how the final core mass changes its scaling behaviour with time and other variables across parameter space (cf. equations 35–38), assuming throughout that pebble accretion is in the settling regime (stopping time $\tau \lesssim 1$). See section 2.3.1 for more background.

When the headwind parameter $\zeta = v_{\text{hw}}/v_{\text{Hill}}$ exceeds the accretion radius $b = R_{\text{acc}}/R_{\text{Hill}}$, the accretion velocity is dominated by the headwind velocity: $v_{\text{acc}} \sim v_{\text{hw}}$, which for our disc temperature profile is constant. The accretion radius R_{acc} follows from equating the kick velocity Δv (equation 16) to $v_{\text{acc}}/4$ (OK10):

$$\frac{GM_{\text{core}}}{R_{\text{acc},\text{hw}}^2} \frac{\tau}{\Omega} \sim \frac{v_{\text{hw}}}{4}$$

$$R_{\text{acc},\text{hw}} \sim \left(\frac{4GM_{\text{core}}\tau}{\Omega v_{\text{hw}}} \right)^{1/2}. \quad (\text{A1})$$

This is equivalent to the wind-shearing radius of [Perets & Murray-Clay \(2011\)](#). Under headwind-dominated conditions, $R_{\text{acc},\text{hw}}$ exceeds the particle scale height H_s =

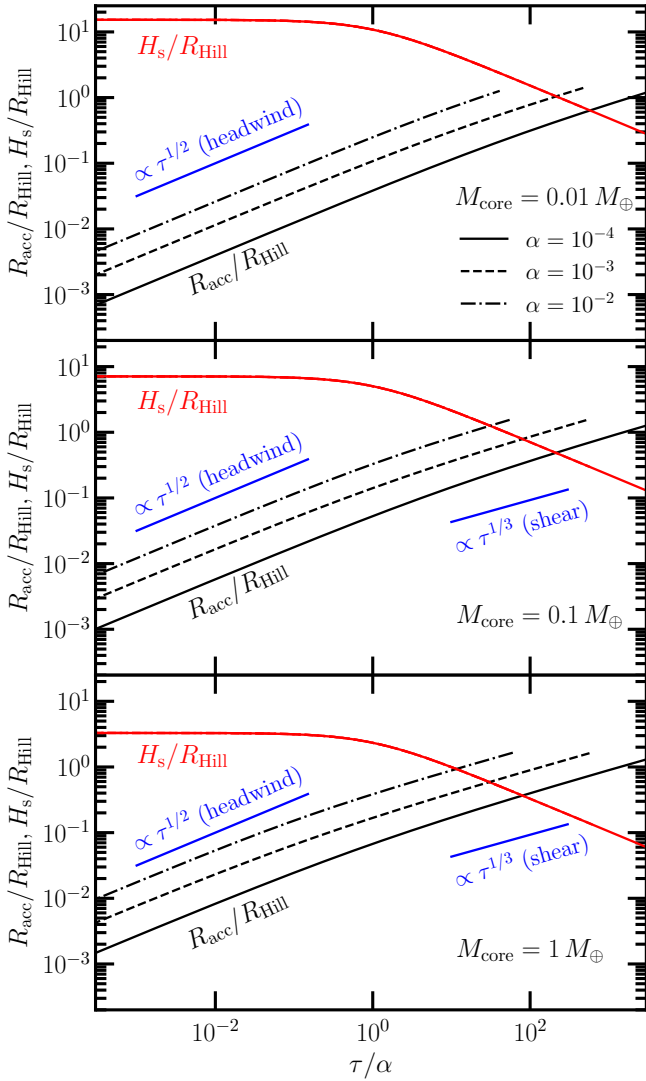


Figure A1. Comparison between the accretion radius R_{acc} (black lines) and the particle scale height H_s (red lines) as a function of the ratio between particle Stokes number (dimensionless stopping time) τ and turbulent Mach number α . We truncate an $R_{\text{acc}}/R_{\text{Hill}}$ curve when pebble accretion ceases to be in the settling regime (i.e., when equation 15 is not satisfied). All values are calculated at $a = 5 \text{ AU}$. At fixed core mass, accretion is headwind-dominated at small τ/α and shear-dominated at large τ/α (compare $R_{\text{acc}}/R_{\text{Hill}}$ curves to blue segments; see equations A1 and A3).

$H\sqrt{\alpha/(\alpha + \tau)}$ when

$$\begin{aligned} \frac{\tau}{\alpha} &> \left(\frac{f_P}{4\alpha}\right)^{1/2} \left(\frac{c_s}{\Omega a}\right)^2 \left(\frac{M_\star}{M_{\text{core}}}\right)^{1/2} \\ &\gtrsim 100 \left(\frac{a}{1 \text{ AU}}\right)^{1/2} \left(\frac{0.01 M_\oplus}{M_{\text{core}}}\right)^{1/2} \left(\frac{0.001}{\alpha}\right)^{1/2} \end{aligned} \quad (\text{A2})$$

where the second inequality follows from our disc parameters: $f_P = 11/8$, $T = 260 \text{ K}(a/1 \text{ AU})^{-1/2}$, and $M_\star = M_\odot$. Technically the above criterion for whether R_{acc} exceeds H_s is derived assuming $\tau > \alpha$, but this is a safe assumption; if $\tau < \alpha$, so that small particles are strongly stirred by gas

turbulence, then only super-massive cores ($\gtrsim 100 M_\oplus$) have accretion radii $R_{\text{acc}} > H_s$.

On the other hand, when $\zeta < b$, the accretion velocity is dominated by the Keplerian shearing velocity $v_{\text{acc}} \sim 3\Omega R_{\text{acc}}/2$. Then

$$\begin{aligned} \frac{GM_{\text{core}}}{R_{\text{acc},\text{sh}}^2} \frac{\tau}{\Omega} &\sim \frac{3\Omega R_{\text{acc},\text{sh}}}{8} \\ R_{\text{acc},\text{sh}} &\sim \left(\frac{8GM_{\text{core}}\tau}{3\Omega^2}\right)^{1/3}. \end{aligned} \quad (\text{A3})$$

The transition from headwind-dominated to shear-dominated accretion (what Lambrechts & Johansen 2012 call drift accretion vs. Hill accretion) occurs when $R_{\text{acc},\text{hw}} \sim R_{\text{acc},\text{sh}}$:

$$\begin{aligned} M_{\text{core,trans}} &\sim v_{\text{hw}}^3 / (9G\Omega\tau) \\ &\sim 0.1 M_\oplus \left(\frac{0.001}{\tau}\right) \left(\frac{a}{1 \text{ AU}}\right)^{3/2}. \end{aligned} \quad (\text{A4})$$

We emphasize that the transition core mass depends on τ (see also equation 7.9 of Ormel 2017). Under shear-dominated conditions, $R_{\text{acc}} > H_s$ when

$$\begin{aligned} \frac{\tau}{\alpha} &> \left(\frac{3}{8\alpha}\right)^{2/5} \left(\frac{c_s}{\Omega a}\right)^{6/5} \left(\frac{M_\star}{M_{\text{core}}}\right)^{2/5} \\ &\gtrsim 30 \left(\frac{a}{1 \text{ AU}}\right)^{3/10} \left(\frac{M_\oplus}{M_{\text{core}}}\right)^{2/5} \left(\frac{0.001}{\alpha}\right)^{2/5} \end{aligned} \quad (\text{A5})$$

where we have again safely assumed $\tau > \alpha$.

Armed with the above relations, we derive the approximate scaling behaviour of the core mass in various regimes. When $R_{\text{acc}} < H_s$, the accretion rate \dot{M}_{core} is identical between headwind and shear-dominated regimes, and is given by equation (35). The accretion rate is the same between these regimes because $\dot{M}_{\text{core}} \propto R_{\text{acc}}^2 v_{\text{acc}}$ (when $R_{\text{acc}} < H_s$), and the combination $R_{\text{acc}}^2 v_{\text{acc}}$ is given in the settling limit by its defining condition, $GM_{\text{core}}/R_{\text{acc}}^2 \times \tau/\Omega \sim v_{\text{acc}}/4$ (Ormel & Klahr 2010). The end result is that $M_{\text{core}}(t)$ is given by equation (36) and is exponential if not super-exponential in time, depending on how Σ_s evolves at the position of the core.

When $R_{\text{acc}} > H_s$, and when accretion is headwind-dominated, $\dot{M}_{\text{core}} = 2\Sigma_s R_{\text{acc},\text{hw}} v_{\text{hw}}$, which together with (A1) yields

$$\dot{M}_{\text{core}} = 4 \left(\frac{v_{\text{hw}}}{\Omega a}\right)^{1/2} \tau^{1/2} \left(\frac{M_{\text{core}}}{M_\star}\right)^{1/2} \Omega \Sigma_s a^2 \quad (\text{A6})$$

and

$$M_{\text{core}}(t) = \left[M_{\text{core}}(0)^{1/2} + 2 \left(\frac{v_{\text{hw}}}{\Omega a}\right)^{1/2} \tau^{1/2} \frac{\Omega a^2}{M_\star^{1/2}} \int_0^t \Sigma_s dt \right]^2 \quad (\text{A7})$$

where all quantities are evaluated at the core's position. When $R_{\text{acc}} > H_s$ and accretion is shear-dominated, $\dot{M}_{\text{core}} = 3\Sigma_s R_{\text{acc},\text{sh}}^2 \Omega$, so that

$$\dot{M}_{\text{core}} = (192)^{1/3} \tau^{2/3} \left(\frac{M_{\text{core}}}{M_\star}\right)^{2/3} \Omega \Sigma_s a^2 \quad (\text{A8})$$

and

$$M_{\text{core}}(t) = \left[M_{\text{core}}(0)^{1/3} + \left(\frac{8}{3}\right)^{2/3} \tau^{2/3} \frac{\Omega a^2}{M_\star^{2/3}} \int_0^t \Sigma_s dt \right]^3. \quad (\text{A9})$$

REFERENCES

- ALMA Partnership et al., 2015, *ApJ*, **808**, L3
- Ali-Dib M., Johansen A., Huang C. X., 2017, *MNRAS*, **469**, 5016
- Andrews S. M., et al., 2012, *ApJ*, **744**, 162
- Andrews S. M., et al., 2016, *ApJ*, **820**, L40
- Batygin K., Bodenheimer P. H., Laughlin G. P., 2016, *ApJ*, **829**, 114
- Birnstiel T., Klahr H., Ercolano B., 2012, *A&A*, **539**, A148
- Bitsch B., Johansen A., Lambrechts M., Morbidelli A., 2015a, *A&A*, **575**, A28
- Bitsch B., Lambrechts M., Johansen A., 2015b, *A&A*, **582**, A112
- Bitsch B., Morbidelli A., Johansen A., Lega E., Lambrechts M., Crida A., 2018, *A&A*, **612**, A30
- Brouwers M. G., Vazan A., Ormel C. W., 2018, *A&A*, **611**, A65
- Buchhave L. A., et al., 2014, *Nature*, **509**, 593
- Chiang E., Laughlin G., 2013, *MNRAS*, **431**, 3444
- Chiang E., Youdin A. N., 2010, *Annual Review of Earth and Planetary Sciences*, **38**, 493
- D'Angelo G., Lubow S. H., 2010, *ApJ*, **724**, 730
- Dawson R. I., Chiang E., Lee E. J., 2015, *MNRAS*, **453**, 1471
- Dawson R. I., Lee E. J., Chiang E., 2016, *ApJ*, **822**, 54
- Dipierro G., Laibe G., 2017, *MNRAS*, **469**, 1932
- Dong R., Fung J., 2017, *ApJ*, **835**, 146
- Duffell P. C., Haiman Z., MacFadyen A. I., D'Orazio D. J., Farris B. D., 2014, *ApJ*, **792**, L10
- Fischer D. A., Valenti J., 2005, *ApJ*, **622**, 1102
- Fung J., Shi J.-M., Chiang E., 2014, *ApJ*, **782**, 88
- Fung J., Artymowicz P., Wu Y., 2015, *ApJ*, **811**, 101
- Ginzburg S., Schlichting H. E., Sari R., 2016, *ApJ*, **825**, 29
- Goldreich P., Schlichting H. E., 2014, *AJ*, **147**, 32
- Goldreich P., Lithwick Y., Sari R., 2004, *ARA&A*, **42**, 549
- Hartmann L., Calvet N., Gullbring E., D'Alessio P., 1998, *ApJ*, **495**, 385
- Ida S., Lin D. N. C., 2008, *ApJ*, **673**, 487
- Izidoro A., Ogihara M., Raymond S. N., Morbidelli A., Pierens A., Bitsch B., Cossou C., Hersant F., 2017, *MNRAS*, **470**, 1750
- Kanagawa K. D., Muto T., Tanaka H., Tanigawa T., Takeuchi T., Tsukagoshi T., Momose M., 2015, *ApJ*, **806**, L15
- Kley W., Nelson R. P., 2012, *ARA&A*, **50**, 211
- Kretke K. A., Levison H. F., 2014, *AJ*, **148**, 109
- Lambrechts M., Johansen A., 2012, *A&A*, **544**, A32
- Lambrechts M., Johansen A., 2014, *A&A*, **572**
- Lambrechts M., Johansen A., Morbidelli A., 2014, *A&A*, **572**, A35
- Lee E. J., Chiang E., 2015, *ApJ*, **811**, 41
- Lee E. J., Chiang E., 2016, *ApJ*, **817**
- Lee E. J., Chiang E., 2017, *ApJ*, **842**, 40
- Lee E. J., Chiang E., Ormel C. W., 2014, *ApJ*, **797**
- Levison H. F., Kretke K. A., Duncan M. J., 2015, *Nature*, **524**, 322
- Lynden-Bell D., Pringle J. E., 1974, *MNRAS*, **168**, 603
- Menu J., et al., 2014, *A&A*, **564**, A93
- Morbidelli A., Lambrechts M., Jacobson S., Bitsch B., 2015, *Icarus*, **258**, 418
- Ogihara M., Kokubo E., Suzuki T. K., Morbidelli A., 2018, preprint, ([arXiv:1804.01070](https://arxiv.org/abs/1804.01070))
- Ormel C. W., 2013, *MNRAS*, **428**, 3526
- Ormel C. W., 2014, *ApJ*, **789**, L18
- Ormel C. W., 2017, The Emerging Paradigm of Pebble Accretion. Springer International Publishing, Cham, pp 197–228, doi:10.1007/978-3-319-60609-5_7, https://doi.org/10.1007/978-3-319-60609-5_7
- Ormel C. W., Klahr H. H., 2010, *A&A*, **520**, A43
- Ormel C. W., Kobayashi H., 2012, *ApJ*, **747**, 115
- Ormel C. W., Liu B., 2018, preprint, ([arXiv:1803.06150](https://arxiv.org/abs/1803.06150))
- Ormel C. W., Liu B., Schoonenberg D., 2017, *A&A*, **604**, A1
- Perets H. B., Murray-Clay R. A., 2011, *ApJ*, **733**, 56
- Pérez L. M., et al., 2015, *ApJ*, **813**, 41
- Petigura E. A., et al., 2018, *AJ*, **155**, 89
- Pinilla P., Youdin A., 2017, Particle Trapping in Protoplanetary Disks: Models vs. Observations. Springer International Publishing, Cham, pp 91–142, doi:10.1007/978-3-319-60609-5_4, https://doi.org/10.1007/978-3-319-60609-5_4
- Piso A.-M. A., Youdin A. N., 2014, *ApJ*, **786**, 21
- Pollack J. B., Hubickyj O., Bodenheimer P., Lissauer J. J., Podolak M., Greenzweig Y., 1996, *Icarus*, **124**, 62
- Popovas A., Nordlund Å., Ramsey J. P., Ormel C. W., 2018, preprint, ([arXiv:1801.07707](https://arxiv.org/abs/1801.07707))
- Powell D., Murray-Clay R., Schlichting H. E., 2017, *ApJ*, **840**
- Rosenthal M. M., Murray-Clay R. A., Perets H. B., Wolansky N., 2018, preprint, ([arXiv:1805.06898](https://arxiv.org/abs/1805.06898))
- Rosotti G. P., Juhasz A., Booth R. A., Clarke C. J., 2016, *MNRAS*, **459**, 2790
- Shakura N. I., Sunyaev R. A., 1973, *A&A*, **24**, 337
- Tazzari M., et al., 2016, *A&A*, **588**, A53
- Tripathi A., Andrews S. M., Birnstiel T., Wilner D. J., 2017, *ApJ*, **845**, 44
- Tripathi A., et al., 2018, preprint, ([arXiv:1805.06487](https://arxiv.org/abs/1805.06487))
- Weidenschilling S. J., 1977, *MNRAS*, **180**, 57
- Xu Z., Bai X.-N., Murray-Clay R. A., 2017, *ApJ*, **847**, 52
- Youdin A. N., Chiang E. I., 2004, *ApJ*, **601**, 1109
- Youdin A. N., Lithwick Y., 2007, *Icarus*, **192**, 588

This paper has been typeset from a Te_X/L_AT_EX file prepared by the author.